AD-A193 404 KINETIC THEORY FOR ELECTROSTATIC WAVES DUE TO TRANSVERSE VELOCITY SHEARS(U) NAVAL RESEARCH LAB WASHINGTON DC G GANGULI ET AL. 22 FEB 88 NRL-MR-6135 1/1

UNCLASSIFIED F/G 20/9 NL

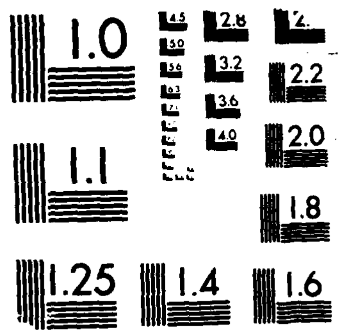

MICROCOPY RESOLUTION TEST CHART

TANDARDS 1963 A

DTIC FILE COPY

(2)

Naval Research Laboratory

Washington, DC 20375-5000

NRL Memorandum Report 6135

AD-A193 404

Kinetic Theory for Electrostatic Waves Due to Transverse Velocity Shears

G. GANGULI,* AND Y. C. LEE† AND P. J. PALMADESSO

**Science Applications International Corporation*
McLean, Virginia 22012

Plasma Physics Division

†University of Maryland
College Park, MD 20742

February 22, 1988

Approved for public release; distribution unlimited.

88 3 14 010

SECURITY CLASSIFICATION OF THIS PAGE

REPORT DOCUMENTATION PAGE

Form Approved OMB No 0704-0188

1a REPORT SECURITY CLASSIFICATION: UNCLASSIFIED	1b RESTRICTIVE MARKINGS
2a SECURITY CLASSIFICATION AUTHORITY	3 DISTRIBUTION/AVAILABILITY OF REPORT: Approved for public release; distribution unlimited.
2b DECLASSIFICATION/DOWNGRADING SCHEDULE	
4 PERFORMING ORGANIZATION REPORT NUMBER(S): NRL Memorandum Report 6135	5 MONITORING ORGANIZATION REPORT NUMBER(S)
6a NAME OF PERFORMING ORGANIZATION: Naval Research Laboratory; 6b OFFICE SYMBOL (If applicable): 4780	7a NAME OF MONITORING ORGANIZATION
6c ADDRESS (City, State, and ZIP Code): Washington, DC 20375-5000	7b ADDRESS (City, State, and ZIP Code)
8a NAME OF FUNDING/SPONSORING ORGANIZATION: ONR and NASA; 8b OFFICE SYMBOL (If applicable)	9 PROCUREMENT INSTRUMENT IDENTIFICATION NUMBER: 47-0883-07 (ONR) 47-1447-07 (NASA)
8c ADDRESS (City, State, and ZIP Code): ONR, Arlington, VA 22203; NASA, Washington, DC 20546	10 SOURCE OF FUNDING NUMBERS: PROGRAM ELEMENT NO 61153N; PROJECT NO W-16, 154; TASK NO RR033-02-44; WORK UNIT ACCESSION NO DN880-024

11 TITLE (Include Security Classification)
Kinetic Theory for Electrostatic Waves Due to Transverse Velocity Shears

12 PERSONAL AUTHOR(S)
Ganguli,* G., Lee,+ Y.C. and Palmadesso, P.J.

13a TYPE OF REPORT	13b TIME COVERED	14 DATE OF REPORT (Year, Month, Day)	15 PAGE COUNT
Interim	FROM ____ TO ____	1988 February 22	68

16 SUPPLEMENTARY NOTATION
*Science Applications International Corporation, McLean, VA 22012
+University of Maryland, College Park, MD 20742

17 COSATI CODES			18 SUBJECT TERMS (Continue on reverse if necessary and identify by block number)
FIELD	GROUP	SUB-GROUP	Kinetic, Kelvin-Helmholtz, Instability, Nonlocal, Ion-cyclotron-like

19 ABSTRACT (Continue on reverse if necessary and identify by block number)

A kinetic theory in the form of an integral equation is provided to study the electrostatic oscillations in a collisionless plasma immersed in a uniform magnetic field and a nonuniform transverse electric field. In the low temperature limit ($k_y \rho_i << 1$, where k_y is the wave vector in the y direction and ρ_i is the ion gyroradius) we recover the dispersion differential equation for the transverse Kelvin-Helmholtz modes for arbitrary values of $k_{||}$, where $k_{||}$ is the component of the wave vector in the direction of the external magnetic field assumed in the z direction. For higher temperatures ($k_y \rho_i > 1$) we recover the ion-cyclotron-like modes described earlier in the literature by Ganguli, Lee and Palmadesso. In this article we reduce the integral equation to a second order differential equation and study the kinetic Kevin-Helmholtz and the ion cyclotron-like modes which constitute the two branches of oscillation in a magnetized plasma including a transverse inhomogenous d.c. electric field.

20 DISTRIBUTION/AVAILABILITY OF ABSTRACT: ☒ UNCLASSIFIED/UNLIMITED ☐ SAME AS RPT ☐ DTIC USERS	21 ABSTRACT SECURITY CLASSIFICATION: UNCLASSIFIED
22a NAME OF RESPONSIBLE INDIVIDUAL: J. D. Huba	22b TELEPHONE (Include Area Code): 202 767-3630; 22c OFFICE SYMBOL: 4780

DD Form 1473, JUN 86 Previous editions are obsolete SECURITY CLASSIFICATION OF THIS PAGE

CONTENTS

KINETIC THEORY FOR ELECTROSTATIC WAVES DUE TO TRANSVERSE VELOCITY SHEARS

INTRODUCTION

Shear in the flow velocity of a fluid leads to the low frequency and long wavelength Kelvin-Helmholtz (K-H) instability[1]. The velocity shear can be generated in a number of ways. In a plasma the existence of an inhomogeneous electric field component transverse to the ambient uniform magnetic field can provide a transverse velocity shear. The evolution of the K-H instability in this configuration has been extensively studied[2].

Recently some space observations[3] and laboratory experiments[4] seem to indicate that ion-cyclotron-like waves are observed for subcritical field aligned currents and therefore the origin of these waves are somewhat mysterious. A crucial feature of these observations and experiments was the presence of a transverse component of a zero order electric field. In order to study the role of the transverse electric fields in the generation of the ion-cyclotron-like waves[3,4] we suggested a mechanism based on the coupling of the negative energy ion Bernstein modes (or the ion cyclotron modes) in the region where the d.c. electric field is localized, with the positive energy ion Bernstein modes (or the cyclotron modes) in the region where the d.c. electric field is absent[5]. This is similar to the negative energy wave growth in an inhomogeneous mirror geometry[6]. In our initial theory we idealized a typical electric field profile by a piecewise continuous function for simplicity. The gradients of the electric field were ignored so as to avoid the K-H modes for which the second derivative of the electric field is necessary. Here we use kinetic theory to obtain the general dispersion relation rigorously, for the electrostatic oscillations in a plasma, in the form of an integral equation for an arbitrary electric profile. In various limits we reduce the integral equation to second order differential equations to obtain the eigenvalues. The integral equation will be solved in a subsequent paper.

Manuscript approved October 2, 1987.

THEORY

The equation of motion of a charged particle in a uniform magnetic field in the z direction and a nonuniform electric field in the x direction is given by

$$\frac{d^2}{dt^2}\underline{r} = \frac{e}{m}E(x)\hat{x} + \Omega\,\underline{v} \times \hat{z}, \tag{1}$$

where $\Omega = eB_o/mc$ is the gyrofrequency, e, m and B_o are the charge, mass and the ambient uniform magnetic field. The constants of the motion are (i) $H = (v_x^2 + v_y^2 + v_z^2)/2 + e\Psi(x)/m$, the total energy, where $E(x) = -\partial\Psi(x)/\partial x$; and (ii), $X_g = x + v_y/\Omega$, which is obtained by integrating the y component of (1). Using $v_y = \Omega(X_g - x)$ in the expression for H we obtain the Hamiltonian for an equivalent one dimensional problem,

$$H = v_x^2/2 + \Omega^2(X_g - x)^2/2 + \frac{e}{m}\Psi(x) . \tag{2}$$

Minimizing the potential of (2) we obtain the guiding center position

$$\xi = x + \frac{v_y - V_E(\xi)}{\Omega} , \tag{3}$$

another constant of the motion which is an implicit function of X_g and therefore is not an independent constant of motion. Here $V_E(\xi)=-cE(\xi)/B_o$.

In order to recover the fluid K-H modes as the fluid limit of the kinetic formalism, we will need to construct an equilibrium distribution function using the constants of motion, such that the equilibrium density is uniform or nearly so. However, we would also like to be able to study the more general case of an equilibrium with an arbitrary density profile. Therefore, we will choose the distribution function to be of the form

$f_0(\xi,H) = n_0(\xi)F_0(\xi,H)$, such that $\int F_0 d^3v \approx$ constant. Then we obtain an appropriate f_0 for the study of the classical K-H mode by setting $n_0(\xi)$ = constant, and an appropriate f_0 for the general case by relaxing this condition. Such a distribution function which leads to an equilibrium density uniform to $O(\varepsilon)$ for a constant n_0, where ε $(=\rho_i/L)$ is the smallness parameter, ρ_i $(=v_{ti}/\Omega_i)$ is the ion gyroradius and L is the characteristic length associated with the external electric field can be found by a systematic procedure and is given by,

$$f_o(\xi, H) = N \exp\left[-\beta H\right] g(\xi), \tag{4}$$

where $N = n_o(\beta/2\pi)^{3/2}$, $\beta = 1/v_t^2$, v_t is the thermal velocity and,

$$g(\xi) = \exp\left[\beta\{e\Psi(\xi)/m + V_E^2(\xi)/2\}\right]\eta(\xi)^{-1/2}$$

where $\eta(\xi) = 1 + V_E'(\xi)/\Omega$. The quantity η parameterizes the magnitude of the velocity shear. Note that there are two crucial parameters in this problem; (i) η and (ii) ε. We will allow η to be arbitrary but positive while assuming $\varepsilon << 1$. The equilibrium distribution can be expressed as,

$$f_o(\xi,H) = \frac{N \exp(-\frac{\beta}{2} w_\perp^2)\exp(-\frac{\beta}{2} v_z^2)}{\sqrt{\eta(\xi)}}, \tag{5}$$

where we have expanded the x dependence of (4) around ξ and neglected terms of $O(\varepsilon^3)$ and higher. Here $w_\perp^2$ is,

$$w_\perp^2 = v_x^2 + \eta(\xi)u_y^2 + \frac{V_E''(\xi)}{\Omega^2}\left(u_y\langle u_y^2\rangle - \frac{u_y^3}{3}\right). \tag{6}$$

where $u_y = v_y - \langle v_y \rangle$ and "< >" indicates time average.

Integrating (5) over all velocities we can show that the equilibrium density distribution $n = n_0\{ 1 + o(\varepsilon^2) \}$, is uniform to order ε. It is possible to devise a distribution function with density uniform to any desired higher order in ε, but this is not necessary here. For generality, in the following we shall consider a nonuniform equilibrium density profile, i.e. $n_0 = n_0(\xi)$.

Now using the definitions,

$$\phi(r', t') = \exp\{-i(\omega t' - k_y y')\}\phi(x') \tag{7a}$$

$$\phi(x') = \int dk_x' \exp(ik_x' x')\phi(k_x') \quad , \tag{7b}$$

where ϕ is the electrostatic potential for the perturbed electric field and linearizing the Vlasov equation, we obtain the perturbed distribution function

$$f_1(x, \underline{v}) = -\beta\frac{e}{m}f_o\left[\int dk_x' \exp\{i(k_x' x)\}\phi(k_x') + i\int dk_x'\phi(k_x')(\omega - k_y V_g)\int_\infty^t dt' A\right] \; , \tag{8}$$

where, $\tau = t' - t$,

$$A(t',x',y',z') = \exp\left\{i(k_x' x' + k_y(y' - y) + k_z(z'-z) - \omega\tau)\right\} , \tag{9}$$

$$V_g(\xi) = \frac{1}{\beta\eta(\xi)f_o\Omega}\frac{\partial f_o}{\partial\xi} = V_E(\xi) - \frac{V_E''(\xi)\rho^2}{2\eta^2} + \frac{\varepsilon_n\rho\Omega}{\eta} \quad . \tag{10}$$

Here $\varepsilon_n = \rho/L_n$, and $L_n = ((dn_0(\xi)/d\xi)/n_0(\xi))^{-1}$ is the scale length associated with the equilibrium density profile. In order to evaluate the time integral in (8) we need the orbits. The x component of (1) gives the net force in this direction. Since v_x is oscillatory in equilibrium, $\langle \dot{v}_x \rangle = 0$. This leads to the expression for an average equilibrium drift $\langle v_y \rangle = \langle V_E(x) \rangle$ in the y direction. Now expanding V_E around ξ we obtain,

$$\langle v_y \rangle = V_E(\xi) + \frac{V_E''(\xi)}{2\Omega^2 \eta(\xi)} \langle (v_y - V_E(\xi))^2 \rangle + O(\varepsilon^3) \ . \qquad (11)$$

Transforming the equation of motion (1) into a frame moving with $\langle v_y \rangle$ in y direction (i.e., $v_y \rightarrow u_y = v_y - \langle v_y \rangle$) and to the spatial coordinate ξ (i.e. $x \rightarrow \xi$) we obtain the transformed equations of motion,

$$\dot{v}_x = \Omega\eta(\xi) u_y + \frac{V_E''(\xi)}{2\Omega} \left(\langle u_y^2 \rangle - u_y^2 \right) \ ; \quad \dot{u}_y = - \Omega v_x \quad , \qquad (12)$$

where we have neglected terms of $O(\varepsilon^3)$ and higher. These equations lead to (see Appendix I),

$$v_x = w_\perp \operatorname{Sin}\Phi - \frac{\hat{w}}{6\eta^{3/2}} \operatorname{Sin}2\Phi \ , \qquad (13a)$$

$$u_y = \frac{w_\perp}{\sqrt{\eta}} \operatorname{Cos}\Phi - \frac{\hat{w}}{12\eta^2} \operatorname{Cos}2\Phi \quad , \qquad (13b)$$

and

$$x' - x = - \frac{w_\perp}{\sqrt{\eta}\,\Omega} \left\{ \operatorname{Cos}\left(\sqrt{\eta}\,\Omega\tau + \Phi\right) - \operatorname{Cos}\Phi \right\} + \frac{\hat{w}}{12\eta^2\Omega} \left\{ \operatorname{Cos}\left(2(\Phi + \sqrt{\eta}\,\Omega\tau)\right) - \operatorname{Cos}2\Phi \right\}, \qquad (14a)$$

$$y'-y = \frac{w_\perp}{\eta\Omega}\left\{\mathrm{Sin}(\Phi+\sqrt{\eta}\Omega\tau) - \mathrm{Sin}\Phi\right\} - \frac{\hat{w}}{24\eta^{5/2}\Omega}\left\{\mathrm{Sin}\left(2(\Phi+\sqrt{\eta}\Omega\tau)\right) - \mathrm{Sin}2\Phi\right\} + \langle v_y\rangle\tau, \quad (14b)$$

$$z'-z = v_z\tau \,, \quad (14c)$$

where $w_\perp{}^2 = v_x{}^2 + \eta(\xi)u_y^2 + V_E''(\xi)\{\langle u_y{}^2\rangle u_y - u_y{}^3/3\}/\Omega^2$, and $\hat{w} = V_E''(\xi)w_\perp{}^2/\Omega^2$. Also $\Phi = \sqrt{\eta}\Omega t + \bar{\Phi}$ where $\bar{\Phi}$ is the velocity space angle at t=0. The oscillatory terms of the order $\hat{w}$ in the orbits are not important except in the derivation of the Jacobian of transformation from the integration variables (x, v_x, v_y) to $(\xi, w_\perp, \Phi)$ which will be necessary in the following. For simplicity therefore, we shall ignore the oscillatory terms of $O(\hat{w})$ everywhere except in the derivation of the Jacobian. This restriction can easily be relaxed.

Using (13) and (14) in (8) we obtain

$$f_1(x,\underline{v}) = -\beta \frac{e}{m} f_o(\xi,H)\left[\int dk_x' \exp\{ik'_x x\}\phi(k_x')\right.$$

$$\left. -\int dk_x' \;\phi(k_x') \sum_{n'} \frac{J_{n'}(\sigma')\;(\omega - k_y V_g)\exp\left(i\left[n'(\Phi - \alpha') + k_x'\bar{\xi} - \frac{k_y w_\perp}{\eta\Omega}\mathrm{Sin}\Phi\right]\right)}{\left(\omega - \sqrt{\eta}\, n'\Omega - k_y \langle v_y\rangle - k_z v_z\right)}\right] \quad (15)$$

where $\sigma' = k_\perp' w_\perp/\Omega$, $k_\perp'^2 = k_x'^2/\eta + k_y^2/\eta^2$, $\alpha' = \tan^{-1}(k'_x\sqrt{\eta}/k_y)$, $\bar{\xi} = x + u_y/\Omega$ and $J_{n'}$ are Bessel functions. The projection of (15) in k_x is

$$f_{1k_x}(\underline{v}) = -\beta \frac{e}{m} \int dk_x' \, \phi(k_x') \int dx \, f_0 \left[\exp\{-i(k_x - k_x')x\} \right.$$

$$\left. - \sum_{n'n} \frac{J_{n'}(\sigma') \, J_n(\sigma)(\omega - k_y V_g)}{\left(\omega - \sqrt{\eta} \, n' \Omega - k_y \langle v_y \rangle - k_z v_z\right)} \exp\left\{ i \left((k_x' - k_x)\bar{\xi} + (n' - n)\Phi + n\alpha - n'\alpha' \right) \right\} \right] \tag{16}$$

The perturbed density is then obtained by integrating the perturbed distribution function over all velocities

$$n_{1k_x} = - \frac{\beta e}{m} \int dv_x dv_y dv_z \int dx \int dk_x' \phi(k_x') f_0 \left[\exp\left(i(k_x' - k_x)x\right) - \exp\left(i(k_x' - k_x)\bar{\xi}\right) F \right] , \tag{17}$$

where,

$$F = (\omega - k_y V_g) \sum_{n',n} \frac{J_{n'}(\sigma') J_n(\sigma)}{\omega - n' \sqrt{\eta} \Omega - k_y \langle v_y \rangle - k_z v_z} \exp\left(i(n' - n)\Phi + n\alpha - n'\alpha'\right) . \tag{18}$$

Equation (17) is the most general form for the perturbed density for either ions or the electrons. In the quasineutral limit the most general dispersion relation for the electrostatic waves, in the form of an integral equation, is given by $\Sigma_\alpha \int \exp(ik_x x) n^\alpha_{1k} dk_x = 0$, where α represents the species.

Now we transform the integration variables in (17) from (x, v_x, v_y) to $(\xi, w_\perp, \Phi)$ using the appropriate Jacobian, which in this case is (see Appendix II) $J = -\sqrt{\eta} w_\perp$; and expand the exponentials in x and $\bar{\xi}$ around ξ and retain terms up to $O(\varepsilon^2)$ to obtain.

$$n_{1k_x} = \frac{Ne\beta}{m}\int_{-\infty}^{+\infty} d\xi \int dv_z \int_0^{\infty} dw_\perp \int_0^{2\pi} d\Phi\sqrt{\eta}w_\perp \int_{-\infty}^{+\infty} dk_x'\phi(k_x')\,\frac{\exp\left(-\beta(w_\perp^2+v_z^2)/2\right)}{\sqrt{\eta}}\exp\left(i(k_x'-k_x)\xi\right)G, \tag{19}$$

where,

$$G = (1-F)\left(1-i(k_x'-k_x)\frac{V_E''(\xi)w_\perp^2}{4\eta^2\Omega^3}\right)-i(k_x'-k_x)\frac{w_\perp \mathrm{Cos}\Phi}{\eta\Omega} - (k_x'-k_x)^2\frac{w_\perp^2\mathrm{Cos}^2\Phi}{2\eta\Omega^2} \quad . \tag{20}$$

We shall first obtain the differential equation for the fluid K-H modes as the fluid limit of (19).

(a) Low Temperature But Arbitrary Shear.

Consider $k_{||}=0$ and $\varepsilon_n=0$. For a quasineutral plasma the condition that the net perturbed density (19) vanishes provides the electrostatic dispersion relation. Further, since $k_{||}=0$ the electron contribution to the net perturbed density is ignorable so that the ion perturbed density set equal to zero leads to the desired general dispersion relation. We shall now proceed to specialize the general dispersion relation for low temperature ($k_y\rho_i \to 0$). Upon Φ integration the term proportional to CosΦ in G, vanishes and n′ becomes n in (18). Since low temperatures are of interest we keep $n=0,\pm1$ terms in F. Higher harmonics are associated with higher orders in temperature. The argument of the Bessel functions can be written as $\sigma=(w_\perp/v_t)(k_\perp L)\varepsilon$ and, assuming that the factors $(k_\perp L)$ and $(w_\perp/v_t)$ are less than or of order unity, we can expand the Bessel functions to $O(\varepsilon^2)$ so that,

$$1-F = 1-\left[1+\frac{k_y(\langle v_y\rangle - V_g)}{\omega_1} - \frac{k_y^2 w_\perp^2}{2\eta^2\Omega^2}\left(1-\frac{\omega_1^2}{\omega_1^2-\eta\Omega^2}\right) - \right.$$

$$\left.\frac{w_\perp^2}{4\eta\Omega^2}\left\{k_x'^2+k_x^2-\frac{2\omega_1{}^2 k_x k_x'}{\omega_1{}^2-\eta\Omega^2}+\frac{2ik_y\omega_1\Omega(k_x'-k_x)}{\omega_1{}^2-\eta\Omega^2}\right\}\right] \quad . \tag{21}$$

It is important to note that under these conditions the terms of order unity in (1-F) drop out. Therefore, the term proportional to $\langle v_y\rangle - V_g = V_E''(w_\perp{}^2/2\Omega^2+\rho_i{}^2)/2\eta^2 \sim O(\varepsilon^2)$, which is responsible for the K-H instability, along with the other terms of the same order, are the leading terms of (19). This will lead to the dispersion differential equation (22), describing the K-H modes. However, when $\sigma \sim O(1)$, the Bessel functions can no longer be expanded and consequently the role of the $O(\varepsilon^2)$ terms, and in particular the V_E'' term, will diminish in importance. This situation, which corresponds to cases in which $k_y\rho_i \gtrsim O(1)$ (ε may still be small), may lead to a significant change in the character of the mode, and possibly to finite gyroradius stabilization of the K-H instability.

In order to obtain the dispersion differential equation for the K-H modes we need to obtain $n_1(x)=\int n_{1kx} \exp(ik_x x)dk_x$, for the ions and set it equal to zero. After carrying out the $w_\perp$ integration, $\rho_i{}^2$ can be factored out and the resulting equation becomes temperature independent in the $\rho_i \to 0$ limit. The k_x integration provides a delta function, $2\pi\delta(x-\xi)$, which makes the ξ integration trivial and converts the ξ dependence into x dependence. Thus, performing the ξ integration after using $\int dk'_x \phi(k_x')\exp(ik'_x\xi) = \phi(\xi)$, we obtain the second order differential equation for the K-H modes in the zero temperature limit.

$$\left\{ \frac{d^2}{dx^2} - A(x)\frac{d}{dx} - B(x)k_y^2 - \frac{k_y V_E''(x)}{\omega_1} C(x) \right\} \phi(x) = 0 \quad , \tag{22}$$

where,

$$A(x) = \frac{2k_y V_E'(x)\omega_1 + \eta'(x)\Omega^2}{\omega_1^2 - \eta(x)\Omega^2} \quad , \tag{23}$$

$$B(x) = 1 + \frac{2(\eta(x)-1)\Omega^2}{\omega_1^2 - \eta(x)\Omega^2} \quad , \tag{24}$$

$$C(x) = \frac{\Omega^2}{\omega_1^2 - \eta(x)\Omega^2} \quad , \tag{25}$$

and $\omega_1 = \omega - k_y V_E(x)$. Equation (22) is the dispersion differential equation for the fluid K-H modes valid for arbitrary shear strength i.e., for arbitrary values of V_E'/Ω_i as long as $\eta > 0$. Starting from the fluid equations one can also derive (22). It should be noted however, that when η becomes small, the arguments of the Bessel functions become large. Thus for $\eta \to 0$ the expansion of the Bessel functions for large argument may not be a good approximation unless the ion temperatures and hence ρ_i also becomes vanishingly small. Thus if η is considered arbitrary then the fluid theory is valid only when $\eta > 0$ and the arguments of the Bessel functions are sufficiently small.

Pritchett and Coroniti[7] used the fluid theory to obtain the dispersion equation for the K-H modes for warm plasmas. They incorporated the temperature effects through the pressure tensor and arrived at equation (16) of reference (7) as the dispersion differential equation. If the temperature related terms (which are included in the factor R in their paper) are set equal to zero in equation (16) of their paper[7], then it reduces to our equation (22). At this stage, by defining a transformation

$U=(\omega_1\phi'-k_y\Omega\phi)/D$ where $D=\eta-(\omega_1/\Omega)^2$, it can be shown that all the η related terms can be transformed away and (22) can be expressed in the form of (34), which represents the classical K-H mode except that $\phi(x)$ is replaced by U. Thus, although the eigenfunctions are affected, the eigenvalues of the classical K-H modes remain unaffected by the magnitude of the velocity shear in the zero temperature limit. This is physically satisfying, since if the gyroradius is zero and in the absence of an equilibrium x drift, particles cannot sample the x direction and hence can not experience the velocity shear irrespective of its magnitude. However, for finite temperatures, the magnitude of the velocity shear will play a role as evidenced in the simulation results[7] and the experimental results of Jassby[8]. Unfortunately in the simple model for the temperature assumed in the reference (7) this cannot be explained since all the temperature related terms can also be transformed away[7]. For arbitrary shears the temperature correction to the lowest order involves a great many terms and will be discussed in a subsequent paper. Here we make the weak shear approximation but treat temperature to be arbitrary and find that the finite gyroradius stabilization of the k-H modes can be understood and predicted by the kinetic theory.

(b) Weak Shear But Arbitrary Temperature.

Now we consider the limit where the shear is not strong but temperature and $k_{||}$ are arbitrary. In this limit, since the the x dependence of the equilibrium quantities are weak, we can assume $k_x \simeq k_x'$ in (20) so that G=1-F. Also for weak shears, $\eta \sim 1$ will be considered. For generality we will also include an equilibrium density profile $N(\xi)$. The perturbed density after carrying out the Φ integration becomes,

$$n_{1\alpha}(x) = \frac{2\pi e_\alpha \beta_\alpha}{m_\alpha} \int_{-\infty}^{+\infty} dk_x \exp\left(ik_x x\right) \int_{-\infty}^{+\infty} d\xi \int_0^{+\infty} dw_\perp w_\perp \int_{-\infty}^{+\infty} dv_z \int_{-\infty}^{+\infty} dk_x' \Phi(k_x') N_\alpha(\xi) \exp\left(i(k_x'-k_x)\xi\right) .$$

$$.\exp\left(-\frac{\beta}{2}(w_\perp^2+v_z^2)\right)\left\{1-\sum_n \frac{(\omega_1+\omega_{2\alpha}-\omega_\alpha^*)\,J_n^2(\sigma_\alpha)}{\omega_1-\omega_{2\alpha}-n\Omega_\alpha-k_z v_z}\right\}, \qquad (26)$$

Here α denotes the species and $\omega - k_y V_{g\alpha} = \omega_1 + \omega_{2\alpha} - \omega^*_\alpha$ where $\omega_{2\alpha} = k_y V_E'' \rho_\alpha^2/2$ and $\omega^*_\alpha = k_y \varepsilon_{n\alpha}\rho_\alpha \Omega_\alpha$. In the denominator we have approximated $\omega - k_y\langle v_y\rangle \simeq \omega_1 - \omega_2$, thereby replacing $w_\perp^2$ by its average value $2v_{t\alpha}^2$. Now the $w_\perp$ and the v_z integrations can easily be performed to yield,

$$n_{1\alpha}(x) = \frac{e_\alpha \beta_\alpha}{m_\alpha} \int_{-\infty}^{+\infty} dk_x \exp(ik_x x) \int_{-\infty}^{+\infty} d\xi\, n_0(\xi) \int_{-\infty}^{+\infty} dk_x' \Phi(k_x') \exp\left(i(k_x'-k_x)\xi\right) .$$

$$.\left\{1+\sum_n \left(\frac{\omega_1+\omega_{2\alpha}-\omega_\alpha^*}{\sqrt{2}|k_{||}|v_{t\alpha}}\right) Z\left(\frac{\omega_1-\omega_{2\alpha}-n\Omega_\alpha}{\sqrt{2}|k_{||}|v_{t\alpha}}\right)\Gamma_n(b_{1\alpha})\right\}, \qquad (27)$$

where $\Gamma_n(b)=I_n(b)\exp(-b)$, and I_n are the modified Bessel functions and $Z(\zeta)$ are the plasma dispersion functions. Here $b_1=\rho_\alpha^2(k_x^2+k_y^2)$. We can expand Γ_n in $k_x^2\rho_\alpha^2$ so that $\Gamma_n(b_1) \sim \Gamma_n(b)+\Gamma_n'(b)k_x^2\rho_\alpha^2+\ldots$, where $\Gamma_n'=d\Gamma_n/db$ and $b=k_y^2\rho_\alpha^2$. Since we have consistently retained terms up to ε^2, we neglect the terms $O(k_x^4\rho_\alpha^4)$ and higher which are of higher order in ε. Using this expansion for $\Gamma_n(b_1)$ in (27) we perform the remaining intergals to obtain,

$$n_{1\alpha}(x)=\frac{1}{2\lambda_\alpha^2 e_\alpha}\left(-\sum_n\left(\frac{\omega_1+\omega_{2\bar{\alpha}}-\omega^*}{\sqrt{2}\,|k_{||}|v_{t\alpha}}\right)Z\left(\frac{\omega_1-\omega_{2\bar{\alpha}}-n\Omega_\alpha}{\sqrt{2}\,|k_{||}|v_{t\alpha}}\right)\rho_\alpha^2\,\Gamma_n'(b_\alpha)\,\frac{d^2}{dx^2}\right.$$

$$\left.+\,1+\sum_n\left(\frac{\omega_1+\omega_{2\bar{\alpha}}-\omega_\alpha^*}{\sqrt{2}\,|k_{||}|v_{t\alpha}}\right)Z\left(\frac{\omega_1-\omega_{2\bar{\alpha}}-n\Omega_\alpha}{\sqrt{2}\,|k_{||}|v_{t\alpha}}\right)\Gamma_n(b_\alpha)\right)\phi(x)\ , \qquad (28)$$

where $\lambda_\alpha{}^2=m_\alpha v_{t\alpha}{}^2/4\pi n_{0\alpha}e_\alpha{}^2$, is the Debye length for the species α. The quasineutrality condition $|e|(n_{1i}-n_{1e})=0$, leads to the general dispersion differential equation for the electrostic modes in the low shear limit. Retaining only the n=0 term for the electrons and considering $\rho_e{}^2<<\rho_i{}^2$ we obtain,

$$\left\{\rho_i^2 A(x)\,\frac{d^2}{dx^2}+Q(x)\right\}\phi(x)=0\ , \qquad (29)$$

where,

$$A(x) = -\sum_n\left(\frac{\omega_1+\ \omega_2-\ \omega^*}{\sqrt{2}\,|k_{||}|v_i}\right)Z\left(\frac{\omega_1-\ \omega_2-n\Omega_i}{\sqrt{2}\,|k_{||}|v_i}\right)\Gamma_n'(b)\ , \qquad (30)$$

and,

$$Q(x) = 1 + \sum_n \left(\frac{\omega_1 + \omega_2 - \omega^*}{\sqrt{2}|k_{||}|v_i}\right) Z\left(\frac{\omega_1 - \omega_2 - n\Omega_i}{\sqrt{2}|k_{||}|v_i}\right) \Gamma_n(b) +$$

$$\tau\left\{ 1 + \left(\frac{\omega_1 + \dfrac{\omega_2}{\tau\mu} + \dfrac{\omega^*}{\tau}}{\sqrt{2}|k_{||}|v_e}\right) Z\left(\frac{\omega_1 - \dfrac{\omega_2}{\tau\mu}}{\sqrt{2}|k_{||}|v_e}\right)\right\} . \tag{31}$$

Here $\tau=T_i/T_e$, $\mu=m_i/m_e$ and $b=(k_y\rho_i)^2$. The subscripts on ω_2 and ω^*, which are for the ions, are suppressed.

In order to recover the dispersion differential equation for the K-H modes in the weak shear limit we set $\omega^*=0$, $k_{||}=0$ and retain $n=0,\pm1$ in (30) and (31) so that,

$$A(x) = \left(\frac{\omega_1 + \omega_2}{\omega_1 - \omega_2}\right) \Gamma_0'(b) + \left(\frac{\omega_1^2 - \omega_2^2}{(\omega_1-\omega_2)^2 - \Omega_i^2}\right) 2\Gamma_1'(b) , \tag{32}$$

and,

$$Q(x) = 1 - \left\{ \left(\frac{\omega_1 + \omega_2}{\omega_1 - \omega_2}\right) \Gamma_0(b) + \left(\frac{\omega_1^2 - \omega_2^2}{(\omega_1-\omega_2)^2 - \Omega_i^2}\right) 2\Gamma_1(b)\right\} . \tag{33}$$

Further, if we take the low temperature limit ($k_y\rho_i \ll 1$, thus $\Gamma_0 \sim (1-b)$, $\Gamma_1 \sim b/2$, $\Gamma'_0 \sim -1$, $\Gamma'_1 \sim 1/2$) and low frequency limit ($\omega_1{}^2/\Omega_i{}^2 \ll 1$) in (32) and (33) and substitute these in (29), we recover the starting differential equation for the K-H modes widely used in the literature[2],

$$\left\{ \rho_i^2 \frac{d^2}{dx^2} - k_y^2\rho_i^2 + \frac{k_y V_E''(x)}{\omega_1} \rho_i^2 \right\} \phi(x) = 0 . \tag{34}$$

For higher temperatures ($k_y \rho_i > 1$) the Bessel functions can no longer be expanded and as explained earlier the terms of the order ε^2, such as ω_2, become less important. Neglecting ω_2 with respect to ω_1 and ignoring the density gradient in (30) and (31) we recover the starting equations for the higher frequency ion-cyclotron-like modes[5].

NUMERICAL RESULTS

(i) Kinetic Kelvin-Helmholtz Modes

We now numerically find the eigenvalues of the general dispersion differential equation (29), which is still in the weak shear limit, first in the fluid limit to recover the fluid results for the electric field profile $E(x)=E_0\tanh(x/L)$. We then use the parameters of the simulation[7] to reproduce those elements of the table (1) of Pritchett and Coroniti[7] which are accessible to the weak shear limit of the theory. The differential equation (29) is solved numerically by a shooting code for the complex eigenvalues, ω. We assume WKB nature of the solutions for $x \to \infty$ and as the boundary condition demand that the energy is outgoing. With ϕ_{WKB} and ϕ'_{WKB} specified at the boundaries for an initial eigenvalue ω_0, we use a variable stepsize integrator to obtain ϕ and ϕ' at the origin where the matching condition is examined. If the matching condition is not satisfied a new ω is assumed and the process iterates till the eigenvalue is obtained with the desired accuracy.

To recover the fluid limit we consider $\varepsilon=0.1$, $\varepsilon_n=0$, $\mu=1837$, $\bar{V}_E=(V_E^0/v_i)=1$, $u=k_{||}/k_y=0.0001$ and $\tau=3.5$. For $k_y\rho_i=0.02$, 0.05 and 0.08 we obtain $\gamma L/V_E^0=0.1369$, 0.1868 and 0.1067. These results coincide with the fluid calculations and are consistent with the normalised growth rate against the dimensionless wavenumber plot for the fluid K-H instability provided in figure (2) of reference (7). Thus the fluid results are recovered from the kinetic dispersion relation for the parameter range that are fluidlike.

We now use $\tau=1$, to match the simulation parameters[7]. Also since $\tau=1$. $c_s=\sqrt{2}v_i$ where $c_s^2=2(T_e+T_i)/m_i$. For $\bar{V}_E=\sqrt{2}V_E^0/c_s=0.764$ we find that the eigenvalues of (29) for $k_yL=0.393$ and $\varepsilon=0.19$ and 0.38 are given by $\gamma L/V_E^0=$ 0.188 and 0.191 while the corresponding eigenvalues for $\bar{V}_E=1.513$ are 0.184 and 0.189. Comparing these with the corresponding elements of the table (1) in Pritchett and Coroniti[7] we find that our theory is in agreement with the simulation results[7]. Figures (1a) and (1b) are the eigenfunction and the profile for the external electric field, for $\varepsilon=0.19$ and $\bar{V}_E=0.764$. For moderate shears ($\varepsilon\lesssim0.5$) better agreement with the simulation can be expected if the assumption of weak shear, i.e. $k_x'\approx k_x$, is relaxed. This will be the subject of a future article. Higher shear values however, are inaccessible to the theory at the present simplified differential equation level. For very high shears a dispersion relation in the form of an integral equation as provided in (17), will become necessary. Also, uncertainty in the simulation results is expected for higher shears where η differs significantly from unity (but still positive), unless the initial loading is in accordance with the equilibrium distribution given in (4). When shear is weak and $\alpha_1=\bar{V}_E\varepsilon$ (the peak value of $V_E'(x)/\Omega$) is small, η is close to unity. For low temperatures ($\varepsilon\to0$), the equilibrium distribution function (4) can be reduced to a Maxwellian shifted in the y velocity by the magnitude of the E X B drift which is approximately $V_E(x)$. Such a distribution function was used by Pritchett and Coronoti[7] for the initial loading. While acceptable for small α_1 and especially for low temperatures, this method may lead to significant relaxation of the initial equilibrium for large α_1 thereby affecting the equilibrium parameters substantially. Thus, for large α_1, the interpretation of the final simulation results[7] remain dubious.

We now study a different electric field profile, $E(x)=E_0 \mathrm{sech}^2(x/L)$. Once again, to check the fluid limit we use $\varepsilon=0.1$, $\tau=1$, $\mu=1837$ and $u=0.0001$. Figure (2) is a plot of the growth rates and the real frequency of the K-H modes as obtained from equation (29) (solid lines) against b. The dashed lines are the fluid results provided in Drazin and Howard[9] in their table (1) under sinuous mode. Good agreement can be expected for $\varepsilon \ll 1$. For larger ε however, the ω_2 appearing in the denominator of (32) and (33) can not be treated as negligible. For larger ε, the denominator ω_2 can influence the results by enhancing the growth rates. This important temperature related effect cannot be predicted by the fluid theory including temperature, as given by Pritchett and Coroniti[7].

A two dimensional particle simulation[10] using an appropriate initial distribution function to study the ion-cyclotron-like modes is currently in progress. Ultimately we shall compare the K-H modes with the ion-cyclotron-like modes[5] through numerical simulation as well as through theory. Thus we will use $\mu=100$ which is being used in our simulation[10]. To study the finite gyroradius stabilization of the K-H modes we plot the growth rates normalised by the ion cyclotron frequency Ω_i against b, for various values of u in figure (3). We consider $\tau=3.5$, $\varepsilon=0.43$ and a mild density gradient $\varepsilon_n=-0.05$ centered around $x_{n0}=1.33\rho_i$ such that $\varepsilon_n=-0.05$ for $x_{n0}-\rho_i < x < x_{n0}+\rho_i$ and 0 otherwise and as the d.c. electric field profile we consider $E(x)=E_0 \mathrm{sech}^2(x/L)$ (see figure (4)). The growth rates of the K-H modes are expected to reduce due to the density gradient[11] but with the mild ε_n used here this decrease was not significant. From figure (3) we see that for a given ε the growth rates peak for a particular b. The peak of the spectrum is localized for $b \sim 0.16$ ($k_y \rho_i \sim 0.4$ and $k_y L \sim 0.93$) and is maximum for transverse propagation ($u=0.0001$). As the obliqueness u is increased, there is a sharp decrease in the peak value along with the narrowing of the spectrum. Beyond $u=0.0075$ the growth of the K-H mode is substantially reduced.

(ii) Ion-Cyclotron-Like Modes

Now we consider the case where $k_y \rho_i > 1$. As explained earlier, in this domain we can no longer expand the Bessel functions and consequently the $O(\varepsilon^2)$ terms responsible for the K-H modes play only a minor role. For the range, in which we are now interested, where $k_y \rho_i \sim 3$, we can neglect these terms for convenience. To explain the ion-cyclotron-like modes we first resort to the piecewise continuous field profile[5] (see figure (5)). This is an idealization of the actual field profile and we use it only to demonstrate the principles involved and to obtain a good starting eigenvalue for numerically tracking the eigenvalues for a smooth profile. For a piecewise continuous profile it is trivial to derive the nonlocal dispersion relation. Setting ω_2 and ω^* equal to zeros in (30) and (31), we use (29) as the differential equation for the modes in question. In the region over which the electric field is localized (we shall refer to this region as region I) there is a Doppler shift in the frequency, i.e., $\omega \to \omega_1 = \omega - k_y V_E$, while outside this region where the electric field is nonexistent (region II) there is no shift in the frequency. This is the essential feature distinguishing the two regions. The matching condition of the logarithmic derivatives of the solutions of (29) at the boundary $x=L/2$, provides the nonlocal dispersion relation.

$$-\ \kappa_I \tan(\kappa_I/2\varepsilon) = i\kappa_{II} \quad , \tag{35}$$

where $\kappa_I^{\,2}=Q(\omega_1)/A(\omega_1)$ and κ_{II} is identical to κ_I if ω_1 is replaced by ω. For details we refer to our earlier papers[5]. The dispersion relation was solved[5] for a wide range of parameters to find growing modes distinct from the K-H modes. We first give a physical description for the origin of these modes.

The dispersion relation of the electrostatic ion Bernstein modes is[5],

$$D(\omega) = 1 - \Gamma_0(b) - \sum_{n>0} \frac{2\omega^2}{\omega^2 - n^2\Omega^2}\,\Gamma_n(b) \quad , \tag{36}$$

where $k_{\parallel} \sim 0$ is assumed. The energy density of these modes are,

$$U \propto \omega\,\frac{\partial D}{\partial \omega} = \omega\left(\sum_{n>0} \frac{4\omega\Gamma_n n^2\Omega^2}{(\omega^2 - n^2\Omega^2)^2}\right) = \omega^2\sigma(\omega), \quad \sigma>0. \tag{37}$$

Clearly, these are positive energy waves. Introduction of an uniform electric field in the x direction initiates an E X B drift in the y direction and consequently there is a Doppler shift in the frequency i.e., $\omega\to\omega_1=\omega-k_yV_E$. The energy density in the presence of the Doppler shift is, $U' \sim \omega\omega_1\sigma(\omega_1)$, which can be negative provided $\omega_1<0$. Now if we consider the localized field configuration as shown in figure (5), then it is clear that due to the E X B drift the energy density in the region I becomes negative while it remains positive in regions II. A nonlocal wavepacket can couple these two regions so that a flow of energy from the region I into the region II will enable the wave to grow. Based on this simple picture we can predict some gross features of the instability. As for example, using the wave-kinetic description it is possible to obtain the energy balance condition for the system from which important scalings governing the growth rate can be predicted. The growth of the wave in region I implies a loss of energy from that region. By conservation of energy, this must be the result of convection of energy into region II and any local energy dissipation (S_-) or free energy release (S_+) processes in region I. The rate of growth of the total energy deficit in region I is proportional to the growth rate γ, the wave energy density U_I in region I, and the volume of region I, represented here by the extent in the x direction (L) of region I times a unit area $A_\perp$ in the plane perpendicular to x. The rate of convection through $A_\perp$ is just $V_G U_{II}$, where V_G is the group velocity in the x direction and U_{II} is the wave energy density in region II. We can then write the energy balance condition as,

$$\gamma U_I L A_\perp \simeq (S_+ - S_- - V_G U_{II}) A_\perp \quad , \tag{38}$$

where S_+ and S_- represent the source and the sink in the region I. The eigenvalues obtained from (35) are expected to satisfy the energy condition (38). For the situation presently under consideration we do not have any external source of free energy and since $k_{||} \sim 0$ the natural dampings are absent and therefore $S_+ = S_- = 0$. Now it is clear from (38) that if U_I is negative then γ can be positive and hence the growth of the wave is sustained by convection of energy into the region II from the region I. On the other hand if U_I is positive then the convection of energy out of the region I would lead to a negative growth rate and therefore to damping of the waves. For $S_\pm = 0$, an important scaling can be predicted from (38) i.e., $\gamma / V_G \propto 1/L$ which with proper normalizations can be written as $\mathrm{Im}(k_x \rho_i) \propto \varepsilon$.

In figure (6) we plot $\mathrm{Im}(k_x\rho_i)$ against ε and confirm this scaling. In figure (6) other parameters are; $\bar{V}_E=2.9$, $\tau=1$, $u=0.0001$, $\mu=1837$ and the growth rates have been maximised in b.

We shall now study the ion-cyclotron-like modes for smooth profiles. For this we use an electric field profile given by,

$$E(x) = \frac{E_0}{A\sinh^2(x/a)+1}\quad , \tag{39}$$

where $A=1/\sinh^2(x_0/a)$ and $x_0=L/2$. For $a\to 0$ (39) represents a "Top Hat" profile which reduces to half of it's peak value at $x=x_0$. As a increases the profile becomes smoother and ultimately when $a=x_0/\sinh^{-1}(1)$ which makes $A=1$, the expression (39) reduces to $E(x)=E_0\mathrm{sech}^2(x/a)$. The shooting code used for the determination of the eigenvalues can operate best when the initial guess for the eigenvalue is not too far away from the actual one. Thus it becomes necessary to use (39) so that in the limit $a\to 0$ we have excellent guess values obtained analytically from the nonlocal dispersion relation (35). Starting with the eigenvalue for the $a\to 0$ case we slowly increase a to track the eigenvalues for the profiles with the desired smoothness. For $b\sim 8$ we have to retain $n=0,\pm1,\pm2,\pm3,\pm4,\pm5,\pm6$ harmonics and the associated plasma dispersion functions in (29) which are evaluated numerically; thus the computations for each eigenvalue is CPU time intensive.

In figure (7a)-(7d) we display the transition of the electric field profile from nearly piecewise continuous to smooth for four different values for a. Here $\varepsilon=0.3$. In figure (8a)-(8d) we display the corresponding wavepackets. Other parameters are; $b=8$, $\tau=3.5$, $u=0.011$, $\mu=1837$, $\bar{V}_E=0.6$, $x_{n0}=1.66\rho_i$ and $\varepsilon_n=-0.07$ if $x_{n0}-0.9\rho_i< x <x_{n0}+0.9\rho_i$ and zero

otherwise. The growth rates did not vary much during this transition. For $a=0.1$, 0.707, 1.41 and 1.89 the corresponding growth rates normalised by the ion cyclotron frequency $\gamma/\Omega_i=0.048$, 0.05, 0.037 and 0.031. There is only a 40% reduction in the growth rate from the sharp to smooth profile and initially in going from $a=0.1$ to $a=0.707$ there is a slight increase in the growth rate. This is in contrast to the K-H instability where the growth rates are dependent on the second derivative of the electric field and are therefore very sensitive to the scale size variation.

In figure (9) we provide a plot of the growth rate and the real frequency of the ion-cyclotron-like modes normalised by the ion gyrofrequency as a function of b. Here the profile in (39) is used with $a=1.87$ and the rest of the parameters are identical to figure (8). We find that the instability is peaked around $k_y\rho_i\sim3$ which for $\varepsilon=0.3$ corresponds to $k_yL\sim10$ which is an order of magnitude larger than the corresponding value of the peak for the K-H modes. Further for $u=0.011$ used here, the K-H modes are expected to be non-existent and thus the domain for dominance for the two modes can be quite distinct. This contradicts the conclusion in reference (12) where a simulation based on only one set of parameters obtained from the idealized field profile[5] was used to conclude that the K-H mode will always dominate the ion-cyclotron-like modes. Further the initial loading in the simulation[12] (assumed to be similar to that of reference (7)) is improper since α_1 for the parameters used was extremely large (greater than unity), and consequently the simulation[12] showed a strong relaxation of the initial nonequilibrium velocity profile.

In figure (10) we use the parameters for our simulation[10] (to be discussed in a separate article) i.e., $\mu=100$, $\tau=3.5$, $\varepsilon=0.43$, $u=0.038$, $\varepsilon_n=-0.05$ for $x_{n0}-\rho_i< x <x_{n0}+\rho_i$ and 0 otherwise and $x_{n0}=1.33\rho_i$ to plot the growth rate and the real frequency normalised by the ion gyrofrequency.

Here for completeness we also include the ω_2 term in (29) to compute the growth rates and use exactly the same d.c. electric field and the density profiles as was used to produce figure (3). The inclusion of the ω_2 term does not change the eigenvalue by much. The peak of the spectrum is around $b \sim 14$. In figure (3) we used the same parameters to conclude that the growth rate for the K-H modes are reduced significantly for $u \geq 0.0075$ and the peak of the spectrum is around $b \sim 0.2$. Once again the domain of dominance for the K-H and the ion-cyclotron-like modes are quite distinct.

Finally in figure (11) we provide a plot of the real and imaginary parts of the eigenfrequency ω normalised by the ion gyrofrequency Ω_i as a function of $\bar{V}_E$, the peak value of the equilibrium E X B drift velocity normalised by the ion thermal velocity. Here $b=10$, $\tau=3.5$, $\mu=1837$, $u=0.011$, $\varepsilon=0.3$, $x_{n0}=1.66\rho_i$, $\varepsilon_n=-0.07$ when $x_{n0}-0.9\rho_i < x < x_{n0}+0.9\rho_i$ and 0 otherwise. For the external electric profile we use (39) with $a=1.87$. We see that the real frequency is almost linearly proportional to $\bar{V}_E$ which is in keeping with the experimental results of Sato et al.[4].

DISCUSSION

We have provided a kinetic theory to study the electrostatic waves that can be excited in a collisionless magnetized warm plasma by a transverse velocity shear. For $k_y\rho_i \ll 1$ we recover the fluid K-H modes and when $k_y\rho_i$ is increased we find that the growth rates for the K-H modes are reduced and for large enough $k_y\rho_i$ the K-H instability is completely damped. Further, the growth of the K-H modes is severely affected by the the parallel dynamics. It seems that for a collisionless plasma the K-H modes can grow only for very small $k_\parallel$. As $k_y\rho_i$ becomes of order unity the expansion of the Bessel functions are no longer possible. Consequently the terms of $O(\varepsilon^2)$ responsible for the K-H modes diminish in importance. At this point the large $k_y \rho_i$ ion-cyclotron-like modes dominate. Further, larger $k_{||}$ and density gradients inhibit the classical K-H wave growth while both these effects favor the ion-cyclotron-like waves.

An important feature of the ion-cyclotron-like modes is the fact that the real frequency of these waves are roughly around $k_y V_E^0/2$ (see figures (9) and (11)). This is similar to the K-H waves and therefore the two instabilities cannot be distinguished by the scaling of the real frequency with $k_y V_E$.

The linear dependence of the real frequency of the ion-cyclotron-like modes on the d.c. electric field was not explicitly discussed in our previous papers[5]. This could have contributed to a misunderstanding which led Pritchett[12] to conclude that since the modes in his simulation for $\rho_i/L=0.3$ and for $k_y \rho_i$ 0.47 and 0.94 displayed the linear dependence of the real frequency on the equilibrium flow velocity they could not be the ion-cyclotron-like modes that we have discussed. A similar misunderstanding was also displayed by Sato et al.[4] in discussing their experimental results.

Since the initial electric field profile used in reference (12) was not in equilibrium, the system immediately relaxed (see Appendix-I, condition (A22); here $\alpha_1=(\rho_i/a)\bar{V}_E=(2.4)3=7.2 >> 1$) to what is shown in figure (4) in reference (12) which is much different from the initial profile given in their[12] equation (2). In fact the initial profile is characterized by two scale lengths L and a with a peak value of about $3v_i$ while the final relaxed profile is more like a Gaussian or a $\mathrm{sech}^2(x/L)$ type characterized by only one scale length L and with a peak value of around $2v_i$. Also, as explained[12] the spatial extent L of the electric field increased during the course of the simulation. Conservatively estimating the broadening of L only by 20%, and considering that the final profile is approximately similar to $\mathrm{sech}^2(x/L)$ with $\rho_i/L=0.25$, then the modes at $k_y\rho_i=0.47$ and 0.94 would correspond to $k_yL=1.88$ and 3.76 respectively. These values will be larger if the spatial extent is broadened more than the 20% assumed. As we have shown through the analysis of the kinetic K-H modes and Drazin and Howard[9] through the analysis of the fluid K-H modes for shear profile of the type $\mathrm{sech}^2(x/L)$, the K-H modes are strongly damped for $k_yL>1$ and almost non existent beyond $k_yL\sim2$. Thus, the mode at $k_y\rho_i=0.47$ can be the tail end of the k-H spectrum but the mode at $k_y\rho_i=0.94$ seems to be completely out of the theoretically predicted k-H spectrum and the growth rate in the second mode is higher. Hence, the conclusion based on the simulations of reference (12) that the K-H mode will always dominate over the ion-cyclotron-like modes for a configuration with a localized electric field perpendicular to an external magnetic field is at best dubious. However, we do agree with the other conclusion[12] that the idealized field profile (piecewise continuous) used earlier[5] to demonstrate the physical principles involved is not suitable for simulation purposes and that a strong relaxation from such a profile to a smoother profile is likely. The fact that the piecewise continuous field profile is an idealization was emphasized in our earlier paper[5]. Here we have provided an equilibrium distribution (4), which if properly loaded should ensure a good equilibrium even for moderate shears. Since the equilibrium distribution as provided in (4), is an implicit function of ξ the guiding center position, it is not in a convenient form for initial loading in a particle simulation. For this purpose we will express (4) in terms of the real position x. From the definition (3) for ξ we get,

$$\xi - x = \frac{v_y - V_E(\xi)}{\Omega} \quad . \tag{40}$$

Expanding $V_E(\xi)$ around x we can show iteratively that,

$$\xi - x = \frac{v_y - V_E(x)}{\eta(x)\Omega} - \frac{V_E''(x)}{2\eta^3(x)\Omega^3}(v_y - V_E(x))^2 \ . \tag{41}$$

Comparing (40) and (41) we find that,

$$v_y - V_E(\xi) = \frac{v_y - V_E(x)}{\eta(x)} + 0(\varepsilon^2) \quad . \tag{42}$$

By definition $u_y = v_y - \langle v_y \rangle$ and using (42) along with the expression (11) for $\langle v_y \rangle$, we can express $u_y = (v_y - V_E(x))/\eta(x) - 0(\varepsilon^2)$. Also expanding $\eta(\xi)$ around x it can be shown that $\eta(\xi) = \eta(x) + 0(\varepsilon)$. Using these to express $w_\perp{}^2$ provided in (6), in terms of x we get,

$$w_\perp^2 = v_x^2 + \frac{\left(v_y - V_E(x)\right)^2}{\eta(x)} + 0(\varepsilon\ ) \quad , \tag{43}$$

and therefore the equilibrium distribution expressed in terms of x becomes $f_0 = n_0 f_{0\perp} f_{0\parallel}$ where $f_{0\parallel} = \sqrt{\beta/2\pi}\exp(-\beta v_z{}^2/2)$ and

$$2\pi f_{0\perp} = \frac{\beta \exp\left(-\frac{\beta}{2}\left[v_x^2 + \frac{(v_y - V_E(x))^2}{\eta(x)}\right]\right)}{\sqrt{\eta(x)}} \left(1 + 0(\varepsilon)\right). \tag{43}$$

It should be noted that when expressed in terms of x the η dependence in $w_\perp^2$ changes from multiplying the y component of the velocity, to dividing it. The distribution given in (43) is the zeroth order distribution function. The correction to order ε is given in Appendix-III.

Consider the case where $\alpha_1 = V_0/L\Omega$, the peak value of the quantity V_E'/Ω, is much smaller than unity (weak shear). Now $\eta \rightarrow 1$ and if $O(\varepsilon)$ corrections are to be ignored then (43) becomes a Maxwellian shifted by the magnitude of the E X B velocity in the y direction. Such a distribution was used by Pritchett and Coroniti[7] and is acceptable for weak shears ($\alpha_1 \ll 1$) especially for low temperatures. To find the correction due to α_1, we express $1/\eta(x) = 1 - V_E'/\Omega$ along with the assumption that the temperature of the system will also be affected so that $\beta \rightarrow \beta + \delta\beta$ such that $\delta\beta \sim O(V_E'/\Omega)$. Using these approximations and $\delta\beta = \beta V_E'/2\Omega$ we can express (43) as,

$$f_{0\perp} = \frac{\beta}{2\pi} \exp\left(-\frac{\beta}{2}\left[v_x^2 + (v_y - V_E(x))^2\right]\right)\left[1 + \frac{\beta V_E'(x)}{4\Omega}\left((v_y - V_E(x))^2 - v_x^2\right)\right] \quad (44)$$

The correction term proportional to α_1 was also discussed in the reference (7) but it was not used for the initial loading since it was expected that the system would make the necessary adjustments and that these would be small, as long as $\alpha_1 \ll 1$. Thus as long as α_1 is small the use of a shifted Maxwellian appears to be acceptable, although (44) describes a better initial distribution. For moderate shears, however, the particle loading should be in accordance with (43), otherwise strong relaxation from the initial profile[12] will be inescapable. Such strong relaxation from a nonequilibrium starting condition is invariably accompanied by substantial free energy release, which leads to a dynamic state quite different from the quiet equilibrium essential for simulation of an instability. A further improved initial distribution function with the O(ε) corrections included, is provided in Appendix-III.

It should be remarked that in most of the experiments[4] and space observations[3] there exists a magnetic field aligned current in addition to the transverse localized electric fields. In the case of an oblique double layer the magnetic field aligned current can originate due to the d.c. electric field component in the direction of the magnetic field provided there are some collisions. As for example, in the experiments of Alport et al.[4] the double layer has a component in the direction of the external magnetic field which is larger than the perpendicular component, thereby providing a large magnetic field aligned current also. Further, in some recent space observations[13] ion-cyclotron-like oscillations have been reported in conjunction with simultaneous observation of a perpendicular component of a d.c. electric field and a magnetic field aligned current for situations where the magnitude of the magnetic field aligned current is below the threshold necessary for the excitation of the current driven ion cyclotron instability[14]. A recent study[15] on the effect of the perpendicular electric field on the current driven ion cyclotron instability[14] indicates that the perpendicular component of the electric field can lower the threshold for the current driven ion cyclotron instability. The necessary condition for the current driven ion cyclotron instability is that the parallel phase velocity $\omega/k_{||}$, of the ion cyclotron waves resonate with the parallel electron drift V_d, such that $(\omega-k_{||}V_d)<0$. For subcritical V_d, $(\omega-k_{||}V_d)>0$ and therefore the Landau damping cannot be inverted[14]. For simplicity again consider the idealized field profile as given in figure (5). The introduction of the perpendicular component of the electric field initiates a $E \times B$ drift and consequently there is a Doppler shift in the frequency ω i.e., $\omega \to \omega_1 = \omega - k_y V_E$ in the region I over which the electric field is localized in the perpendicular direction. Now the necessary condition for the onset of the current driven ion cyclotron instability in the region I becomes $(\omega_1-k_{\|}V_d)<0$, which can be satisfied even though $(\omega-k_{\|}V_d)$ remains positive. Thus the threshold value for the magnetic field aligned drift V_d necessary for the onset of the current driven ion cyclotron instability is lowered.

For the cases where there is a magnetic field aligned drift in addition to the transverse localized electric field, the term S_+ in (38) is not zero and can roughly be estimated (using the local theory) to be proportional to $LU_I\gamma_1$, where the local growth rate in the region I, $\gamma_1=-Q_I/Q_{R\omega}$, evaluated at $\omega=\omega_r$. Q_R and Q_I are the real and the imaginary parts of the local dispersion relation identical to the expression given in (31) with ω_2 and ω^* set equal to zero, and $Q_{R\omega}$ is the ω derivative of Q_R. In the ion rest frame the field aligned drift V_d provides an additional Doppler shift in the electron term so that Q_I is proportional to $(\omega_1-k_{\|}V_d)$. Assuming that the field aligned current is also localized within the region I so that $Q_{R\omega}=U_I/\omega_r$ we can write the energy balance condition as,

$$\gamma LA_{\perp}U_I \simeq -(\omega_1-k_{\|}V_d)\omega_r LA_{\perp}-V_G U_{II}A_{\perp} \quad (45)$$

We have neglected the ion Landau and cyclotron dampings. First consider the case where the electric field is not strong enough to make $\omega_1<0$ and therefore $U_I>0$ but ω_1 is less than ω. Since $\omega_1<\omega$ it is possible to have $(\omega_1-k_yV_E)<0$ when $(\omega-k_yV_E)>0$ and hence the first term in the right hand side of (45) provides a growth even for subcritical V_d while the convection leads to damping. Now if $\omega_1<0$ and consequently $U_I<0$, the convection will lead to growth and the first term in the right hand side will contribute to damping. However, if $k_{\|}V_d<0$ (which can be achieved by keeping V_d constant but changing the direction of parallel propagation or vice versa) growth in the region I may be expected from both the right hand terms for $(\omega_1 - k_{\parallel}V_d)>0$. This can be a likely scenario for most of the experiments and space observations involving the ion-cyclotron-like oscillations for an equilibrium that contains a d.c. electric field in addition to a uniform magnetic field. More details will be provided elsewhere.

CONCLUSIONS

Using a kinetic approach we have studied the generation mechanisms for the electrostatic waves in a magnetized warm plasma including a d.c. electric field perpendicular to the external magnetic field. Two distinct generation mechanisms are discussed (i) Kelvin-Helmholtz mechanism and (ii) positive negative energy wave coupling mechanism. The Kelvin-Helmholtz mechanism, first discussed about a century ago[1], depends directly on the second derivative of the d.c. electric field while the other mechanism[5], depends on the inhomogeneity in the energy density of the waves. The K-H instability can dominate for small $k_y\rho_i$ if the propagation is nearly perpendicular. For a collisionless plasma the K-H instability is strongly damped even if $k_{\parallel}$ is a tiny fraction of k_y. In the theory we have shown that the terms responsible for the K-H wave growth are proportional to $V_E''(x)$ and are of order ε^2. Only when $k_y\rho_i \ll 1$ the Bessel functions can be expanded for large argument and the order unity terms drop out thereby making the order ε^2 terms primary which then assures the dominance of the K-H instability. When $k_y\rho_i$ is increased and is of the order of or greater than unity the Bessel functions can no longer be expanded and consequently the order ε^2 terms responsible for the K-H waves can not gain prominence. At this stage inhomogeneous energy density driven modes[5] dominate. Also, the dominance of the K-H modes can be reduced even for small $k_y\rho_i$ if more oblique propagation (larger $k_{||}$) are considered. Here we have also shown that the inhomogeneous energy density driven modes can tolerate larger $k_{||}$. Thus the two modes are quite distinct and depending on the parameter range (system size, temperature, density gradient etc.)one or the other can dominate.

It should be pointed out that while the interpretation of the inhomogeneous energy density driven modes is quite convincing for the "Top Hat" like profiles as evidenced in figure (6), it is not so clear cut for the smooth profiles. As the profile is made smoother additional physics is introduced through various resonances that are now possible since ω_1 can now vary smoothly over a wide range of values as opposed to one constant value in the region I and a different constant value in the region II for the "Top Hat" profile. Geometry related effects can also play a role. It was also noted that as the smoothness of the profile was increased it was necessary to maintain a very small amount of the density gradient in the transition zone in which the electric field is reducing to zero, to preserve the growth rates. This however, makes the model more physical since in actual experiments (e.g. see Alport et al.[4]) a density gradient is present in the transition zone. It appears that the density gradient acts as a catalyst by maintaining the growth rate without much affecting the real frequency, although the exact role that the density gradient plays is yet to be fully appreciated. The important conclusion however, is the fact that besides the K-H instability there is another branch that can also grow with shorter wavelengths and higher frequency in a plasma immersed in a uniform magnetic field with a nonuniform transverse electric field.

Finally we would like to point out that in the small $k_y \rho_i$ limit the integral equation can be exactly reduced to the second order differential equation (22). Thus the second order differential equation level of description to study the nonlocal wave dispersion properties employed in this paper is more accurate for the K-H modes than the ion-cyclotron-like modes that grow for large $k_y \rho_i$. For greater accuracy the eigenvalues of the integral equation which will result by using (17) as the perturbed density, must be obtained. This will be the topic of a future article.

ACKNOWLEDGMENTS

Discussions with Prof. Pradip Bakshi , Dr. Y.Y. Lau and Dr. P.L. Pritchett are gratefully acknowledged. This work is supported by the Office of the Naval Research and the National Aeronautics and Space Administration.

Bibliography

1. Lord Rayleigh, Theory of Sound, Vol-II, Chapter 21, (MacMillan and Co., London, 1896), Reprinted 1940.

2. A.B. Mikhailovoskii, Theory of Plasma Instabilities, Vol. II, p. 141, (Consultants Bureau, New York, 1974).

3. F.S. Mozer, C.W. Carlson, M.K. Hudson, R.B. Torbert, B. Parady, J. Yatteau and M.C. Kelly, Phys. Rev. Lett. 38, 292, (1977);M. Temerin, C. Cattell, R. Lysak, M. Hudson, R.B. Torbert, F.S. Mozer, R.D. Sharp and P.M. Kintner, J. Geophys. Res. 86,11278 (1981).

4. M.R. Nakamura, R. Hatakeyama and N. Sato, Proceedings of the Second Symposium on Plasma Double Layers and related topics, Innsbruck, Austria,1984, p.224; N. Sato, M. Nakamura and R. Hatakeyama, Phys. Rev. Lett. 57,1227 (1986); M.J. Alport, S.L. Cartier and R.L. Merlino, J. Geophys. Res.,91, 1599 (1986).

5. G. Ganguli, Y.C. Lee and P. Palmadesso, Phys. Fluids.,28, 761 (1985); G. Ganguli, P. Palmadesso and Y.C. Lee, Geophys. Res. Lett.,12, 643 (1985); G. Ganguli, Y.C. Lee and P. Palmadesso, Proceedings of the Chapman Conference on Ion Acceleration, Boston, 1985, p.297; P. Palmadesso, G. Ganguli and Y.C. Lee, Proceedings of the Chapman Conference on Ion Acceleration, Boston, 1985, p.301.

6. H.L. Berk, L.D. Pearlstein, J.D. Callen, C.W. Horton and M.N. Rosenbluth, Phys. Rev. Lett., 22, 876 (1969); H.L. Berk, L.D. Pearlstein and J.G. Cordey, Phys. Fluids., 15, 891 (1972).

7. P.L. Pritchett and F.V. Coroniti, J. Geophys. Res., 89, 168 (1984).

8. D.L. Jassby, Phys. Fluids., 15, 1590 (1972)

9. P.G. Drazin and L.N. Howard, Advances in Applied Mechanics, V-7, p-1, (Academic Press, New York, 19[illegible]).

10. K.I. Nishikawa, G. Ganguli and P. Palmadesso, Trans., American Geophysical Union, 68, 401 (1987)

11. P. Satyanarayana, Y.C. Lee and J.D. Huba, Phys. Fluids, 30, 81 (1987).

12. P.L. Pritchett, Phys. Fluids., 30, 272 (1987).

13. B.G. Fejer, R.W. Reed, D.T. Farley, W.E. Swartz and M.C. Kelly, J. Geophys. Res., 89, 187 (1984): J. Providakes, D.T. Farley, W.E. Swartz and D. Riggin, J. Geophys. Res., 90, 7513 (1985).

14. W.E. Drummond and M.N. Rosenbluth, Phys. Fluids., 5, 1507 (1962).

15. G. Ganguli and P.J. Palmadesso, Geophys. Res. Lett., (1988), (to appear).

APPENDIX I

In this appendix we provide the derivation of the particle orbits to $O(\varepsilon^2)$. The x and y component of the equation of motion (1), can be written as,

$$\dot{v}_x = \Omega v_y - \Omega V_E(x) \quad , \tag{A1}$$

$$\dot{v}_y = -\Omega v_x \ , \tag{A2}$$

where $V_E(x) = -cE(x)/B_0$. Expressing (A1) in the guiding centre frame ξ, and retaining terms upto $O(\varepsilon^2)$ we get,

$$\dot{v}_x = \Omega\left(\eta(\xi)\left(v_y - V_E(\xi)\right) - \frac{\left(v_y - V_E(\xi)\right)^2}{2\Omega^2} V_E''(\xi) + O(\varepsilon^3)\right) . \tag{A3}$$

We now transform (A2) and (A3) to a frame moving with a velocity $\langle v_y \rangle$ in the y direction, (i.e. $v_y \to u_y + \langle v_y \rangle$) so that,

$$\dot{v}_x = \Omega\left(\eta(\xi)u_y + \eta(\xi)\left(\langle v_y \rangle - V_E(\xi)\right) - \frac{\left(u_y + \langle v_y \rangle - V_E(\xi)\right)^2}{2\Omega^2} V_E''(\xi)\right) . \tag{A4}$$

An expression for $\langle v_y \rangle$ was given in equation (11) in the text. Replacing v_y by $u_y + \langle v_y \rangle$ in the right hand side of (11), we find that $\langle v_y \rangle - V_E(\xi) = V_E''(\xi)\langle u_y{}^2 \rangle / 2\Omega^2\eta + O(\varepsilon^3)$. Substituting this in (A4) and transforming v_y to $u_y + \langle v_y \rangle$ in (A2), we obtain the equations of motion in the transformed frames to $O(\varepsilon^2)$,

$$\dot{v}_x = \eta(\xi)\Omega u_y + \frac{V_E''(\xi)}{2\Omega}\left(\langle u_y^2\rangle - u_y^2\right) \quad , \tag{A5}$$

$$\dot{u}_y = -\Omega v_x \quad . \tag{A6}$$

Note that for a linear field, $V_E''=0$ and (A5) and (A6) reduces to a form very similar to that of the equations of motion for zero electric field except for the factor $\eta(\xi)$ in (A5). For $V_E''=0$ it is fairly easy to solve the equations of motion and we can obtain $u_y=A\cos\Phi$, where $\Phi=\sqrt{\eta}\Omega\tau+\bar{\Phi}$ and A is proportional to $w_\perp$. Thus for $V_E''\neq 0$ we assume $u_y=A\cos\Phi+B\cos 2\Phi$, where $B=O(\varepsilon^2)$. Differentiating (A6) once and using (A5) for $\dot{v}_x$ we get,

$$\ddot{u}_y = -\Omega\dot{v}_x = -\eta(\xi)\Omega^2 u_y - \frac{V_E''(\xi)}{2}\left(\langle u_y^2\rangle - u_y^2\right) \quad . \tag{A7}$$

Substituting $u_y=A\cos\Phi+B\cos 2\Phi$, in the left and the right hand sides of (A7) we find,

$$\mathrm{LHS} = -\eta(\xi)\Omega^2 A\cos\Phi - 4\eta(\xi)\Omega^2 B\cos 2\Phi \quad , \tag{A8}$$

$$\mathrm{RHS} = -\eta(\xi)\Omega^2 A\cos\Phi - \left(\eta(\xi)\Omega^2 B - \frac{V_E''(\xi)\ A^2}{4}\right)\cos 2\Phi \quad , \tag{A9}$$

where we have neglected terms smaller than $O(\varepsilon^2)$. Comparing the LHS and the RHS we find that,

$$B = -\frac{V_E''(\xi)A^2}{12\eta(\xi)\Omega^2} \quad . \tag{A10}$$

Thus,

$$u_y = A\cos\Phi - \frac{V_E''(\xi)A^2}{12\eta(\xi)\Omega^2}\cos 2\Phi \quad , \tag{A11}$$

$$v_x = -\frac{\dot{u}_y}{\Omega} = \sqrt{\eta}A\sin\Phi - \frac{V_E''(\xi)A^2}{6\sqrt{\eta}\Omega^2}\sin 2\Phi \quad . \tag{A12}$$

The constant A is still undetermined.

After multiplying Equation (A7) by $\dot{u}_y$ it can be written as,

$$\frac{d}{dt}\left\{ \frac{\dot{u}_y^2}{2} + \eta(\xi)\Omega^2 \frac{u_y^2}{2} - \frac{V_E''(\xi)}{2}\left(\frac{u_y^3}{3} - \langle u_y^2\rangle u_y \right) \right\} = 0 \quad . \tag{A13}$$

Using (A6) we can eliminate $\dot{u}_y$ from (A13) and define a constant $w_\perp{}^2$ as,

$$w_\perp^2 = v_x^2 + \eta(\xi)u_y^2 - \frac{V_E''(\xi)}{\Omega^2}\left(\frac{u_y^3}{3} - \langle u_y^2\rangle u_y \right) \quad . \tag{A14}$$

Substituting u_y and v_x from (A11) and (A12) into (A14) and retaining terms up to $O(\varepsilon^2)$ it can be shown that, $A = w_\perp/\sqrt{\eta}$. Thus,

$$v_x = w_\perp \sin\Phi - \frac{V_E''(\xi)w_\perp^2}{6\eta(\xi)^{3/2}\Omega^2}\sin 2\Phi \quad , \tag{A15}$$

$$u_y = \frac{w_\perp}{\sqrt{\eta(\xi)}}\cos\Phi - \frac{V_E''(\xi)w_\perp^2}{12\eta(\xi)^2\Omega^2}\cos 2\Phi \quad . \tag{A16}$$

With the velocities known it is a simple matter to obtain the positions,

$$x' - x = \int_t^{t'} v_x \, dx$$

$$= -\frac{w_\perp}{\sqrt{\eta(x)}\Omega}\left[\cos\Phi' - \cos\Phi\right] + \frac{V_E''(\xi)w_\perp^2}{12\eta(\xi)^2\Omega^3}\left[\cos2\Phi' - \cos2\Phi\right] \quad . \qquad (A18)$$

Rewriting $\Phi' = \sqrt{\eta}\Omega t' + \bar{\Phi} = \sqrt{\eta}\Omega\tau + \Phi$, where $\tau = t' - t$ and $\Phi = \sqrt{\eta}\Omega t + \bar{\Phi}$, we get,

$$x' - x = -\frac{w_\perp}{\sqrt{\eta(\xi)}\Omega}\left\{\cos\left(\sqrt{\eta(\xi)}\Omega\tau + \Phi\right) - \cos\Phi\right\} +$$

$$\frac{\hat{w}}{12\eta(\xi)^2\Omega}\left\{\cos\left(2(\Phi + \sqrt{\eta(\xi)}\Omega\tau)\right) - \cos2\Phi\right\} \quad , \qquad (A19)$$

where $\hat{w} = V_E''(\xi)w_\perp^2/\Omega^2$. Similarly y'-y can also be obtained. It should be noted that when $\eta \leq 0$, the orbits become unstable.

For computer simulations where a distribution of particles is in consideration we can get an order of magnitude restriction necessary for the stability of the orbit of a typical particle (characterized by a velocity v_t, the thermal velocity and a displacement ρ, the gyroradius). From (A3) it is clear that as long as the first term in the right hand side which is of order v_t, is dominant the form of (A3) is,

$$\ddot{\chi} = -\Omega^2\eta(\xi)\chi + \text{corrections} \quad , \tag{A20}$$

where $\chi=(\xi-x)=(v_y-V_E(\xi))/\Omega$. Therefore the restoring force is proportional to the displacement. This ensures periodic orbits which are stable. On the other hand if the second term in the right hand side of (A3), which is proportional to $v_t^2 V_E''(\xi)/\Omega^2$, dominates then (A3) is of the form,

$$\ddot{\chi} = \Omega\frac{V_E''(\xi)}{2}\chi^2 + \text{corrections} \quad . \tag{A21}$$

The restoring force is now proportional to the square of the displacement. Hence, the orbits are no longer periodic and therefore become unstable. Thus as long as the second term of (A3) remain smaller than the first term i.e., $v_t^2 V_E''(\xi)/2\Omega^2 < \eta(\xi)v_t$, we can expect stable orbits for the typical particles. This restriction leads to the condition for stable orbits in a simulation,

$$\frac{\rho}{R(\xi)} < \left(\frac{2v_t\eta(\xi)}{V_E(\xi)}\right)^{1/2} \quad , \tag{A22}$$

where $R(\xi)$ is the local radius of curvature $(=(|V_E(\xi)/V_E''(\xi)|)^{1/2})$. Simplifying (A22) by replacing the guiding center position ξ by the real position x and considering the electric field profiles of the form $V_E(x)=V_E^0 f(x/L)$, we can define $H(x)$ such that.

$$H(x) = \left(\frac{2v_t}{V_E^0} + 2\varepsilon f'(\bar{x})\right)^{1/2} \quad \left(\left|\frac{f''(\bar{x})}{f(\bar{x})}\right|\right)^{1/2} \quad , \tag{A23}$$

where $\bar{x}=x/L$ and $\varepsilon=\rho/L$. In order to have stable orbits so as to avoid (or minimize) relaxation of the initial electric field profile used in a computer simulation, H(x) should be positive for all x. If this condition is violated then the orbits will become unstable and the profile will relax until (A22) is satisfied.

APPENDIX II

In this appendix we evaluate the Jacobian of transformation from the coordinates (x, v_x, v_y) to the coordinates, $(\xi, w_\perp, \Phi)$. This Jacobian can be written as,

$$J = \begin{vmatrix} \left.\frac{\partial x}{\partial \xi}\right|_{w_\perp,\Phi} & \left.\frac{\partial x}{\partial w_\perp}\right|_{\xi,\Phi} & \left.\frac{\partial x}{\partial \Phi}\right|_{w_\perp,\xi} \\ \left.\frac{\partial v_x}{\partial \xi}\right|_{w_\perp,\Phi} & \left.\frac{\partial v_x}{\partial w_\perp}\right|_{\xi,\Phi} & \left.\frac{\partial v_x}{\partial \Phi}\right|_{w_\perp,\xi} \\ \left.\frac{\partial v_y}{\partial \xi}\right|_{w_\perp,\Phi} & \left.\frac{\partial v_y}{\partial w_\perp}\right|_{\xi,\Phi} & \left.\frac{\partial v_y}{\partial \Phi}\right|_{w_\perp,\xi} \end{vmatrix} . \tag{B1}$$

Using the definition of ξ as given in equation (3) in the text we can evaluate the elements of the first row so that,

$$J = \begin{vmatrix} \eta(\xi) - \frac{1}{\Omega}\frac{\partial v_y}{\partial \xi} & -\frac{1}{\Omega}\frac{\partial v_y}{\partial w_\perp} & -\frac{1}{\Omega}\frac{\partial v_y}{\partial \Phi} \\ \frac{\partial v_x}{\partial \xi} & \frac{\partial v_x}{\partial w_\perp} & \frac{\partial v_x}{\partial \Phi} \\ \frac{\partial v_y}{\partial \xi} & \frac{\partial v_y}{\partial w_\perp} & \frac{\partial v_y}{\partial \Phi} \end{vmatrix} , \tag{B2}$$

where we have suppressed the subscripts. Multiplying the last row by $1/\Omega$ and adding it to the first row we get,

$$J = \begin{vmatrix} \eta(\xi) & 0 & 0 \\ \frac{\partial v_x}{\partial \xi} & \frac{\partial v_x}{\partial w_\perp} & \frac{\partial v_x}{\partial \Phi} \\ \frac{\partial v_y}{\partial \xi} & \frac{\partial v_y}{\partial w_\perp} & \frac{\partial v_y}{\partial \Phi} \end{vmatrix} \quad . \tag{B3}$$

Thus the determinant has been considerably simplified and can be expanded as,

$$J = \eta(\xi) \left[\frac{\partial v_x}{\partial w_\perp} \frac{\partial v_y}{\partial \Phi} - \frac{\partial v_x}{\partial \Phi} \frac{\partial v_y}{\partial w_\perp} \right] \quad . \tag{B4}$$

Recall that $v_y = u_y + \langle v_y \rangle$ and using the expressions for v_x and u_y from (A15) and (A16), and using equation (11) from the text for $\langle v_y \rangle$ we get,

$$v_x = w_\perp \sin\Phi - \frac{V_E''(\xi) w_\perp^2}{6\eta(\xi)^{3/2}\Omega^2} \sin 2\Phi \quad , \tag{B5}$$

$$v_y = \frac{w_\perp}{\sqrt{\eta(\xi)}} \cos\Phi + V_E(\xi) + \frac{V_E''(\xi) w_\perp^2}{4\eta(\xi)^2\Omega^2} \left(1 - \frac{\cos 2\Phi}{3} \right) \quad . \tag{B6}$$

The derivatives necessary in (B4) can be easily obtained, and retaining terms up to $O(\varepsilon^2)$ we get,

$$\frac{\partial v_x}{\partial w_\perp} = \sin\Phi - \frac{V_E''(\xi) w_\perp}{3\eta(\xi)^{3/2}\Omega^2} \sin 2\Phi \quad , \tag{B7}$$

$$\frac{\partial v_y}{\partial \Phi} = -\frac{w_\perp}{\sqrt{\eta(\xi)}}\sin\Phi + \frac{V_E''(\xi)w_\perp^2}{6\eta(\xi)^2\Omega^2}\sin 2\Phi \quad , \tag{B8}$$

$$\frac{\partial v_x}{\partial \Phi} = w_\perp \cos\Phi - \frac{V_E''(\xi)w_\perp^2}{3\eta(\xi)^{3/2}\Omega^2}\cos 2\Phi \quad , \tag{B9}$$

$$\frac{\partial v_y}{\partial w_\perp} = \frac{\cos\Phi}{\sqrt{\eta(\xi)}} + \frac{V_E''(\xi)w_\perp}{2\eta(\xi)^2\Omega^2}\left(1 - \frac{\cos 2\Phi}{3}\right) \tag{B10}$$

Using (B7-10) in (B4) we obtain,

$$J = -\sqrt{\eta(\xi)}w_\perp \quad . \tag{B11}$$

APPENDIX III

In this appendix we provide an equilibrium distribution function suitable for initial loading for a particle simulation studing the electrostatic waves due to an equilibrium field configuration containing an uniform magnetic field and a perpendicular component of a nonuniform electric field. We shall include the corrections which are of the order ε but ignore the order ε^2 corrections for the time being. Expanding $\eta(\xi)$ around x we get $\eta(\xi)=\eta(x)+(\xi-x)\eta'(x)+O(\varepsilon^2)$, where $\eta'=V_E''/\Omega$. Using (41) for $(\xi-x)$ we can write down,

$$\eta(\xi) = \eta(x) + \left(\frac{v_y - V_E(x)}{\eta(x)\Omega}\right)\frac{V_E''(x)}{\Omega} + O(\varepsilon^2) \quad . \tag{C1}$$

Also from the expression for u_y given in (A16) we find that the time average $\langle u_y^2\rangle = w_\perp^2/2\eta(\xi)$. Expressed in terms of x, $\langle u_y^2\rangle = w_\perp^2(1-(v_y-V_E(x))V''_E(x)/\eta^2(x)\Omega^2)/2\eta(x)+O(\varepsilon^2)$. Using this and (C1) in the expression for $w_\perp^2$ as provided in (6) we get,

$$w_\perp^2 = v_x^2 + \frac{\left(v_y - V_E(x)\right)^2}{\eta(x)} + \left(v_y - V_E(x)\right)\left(\frac{v_x^2}{2} - \frac{(v_y - V_E(x))^2}{2\eta(x)}\right)\frac{V_E''(x)}{\eta^2(x)\Omega^2} + O(\varepsilon^2). \tag{C2}$$

Using (C2) in the expression for $f_{0\perp}$ and expanding the $O(\varepsilon)$ terms we get,

$$f_{0\perp} = \frac{\beta}{2\pi}\,\frac{\exp\left\{-\frac{\beta}{2}\left(v_x^2 + \frac{(v_y-V_E(x))^2}{\eta(x)}\right)\right\}}{\sqrt{\eta(x)}}\left\{1 - \right.$$

$$\left(v_y - V_E(x)\right)\left[1 + \beta\left(\frac{v_x^2}{2} - \frac{(v_y - V_E(x))^2}{2\eta(x)}\right)\right] \frac{V_E''(x)}{2\eta^2(x)\Omega^2} + O(\varepsilon^2)\Bigg\} . \qquad \text{(C3)}$$

If the $O(\varepsilon)$ term in (C3) is set equal to zero we recover (43). For even greater accuracy it is possible to obtain the $O(\varepsilon^2)$ corrections also.

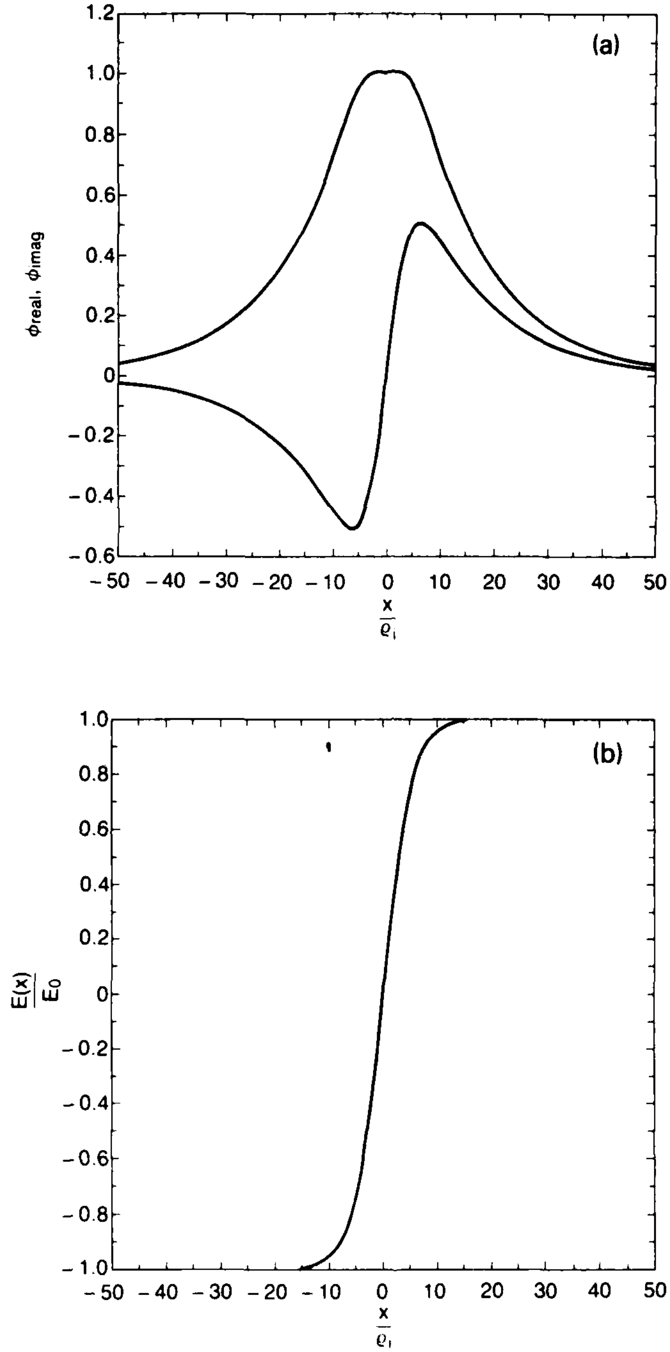

Fig. 1 — (a) Real and imaginary parts of a typical eigenfunction for $E = E_0 \tanh(x/L)$ profile. Here $\epsilon = 0.19$, $k_y \rho_i = 0.074$, $V_E = 0.764$, $\mu = 1837$, $u = 0.0001$ and $\tau = 1$. (b) The external electric field profile for $\epsilon = 0.19$.

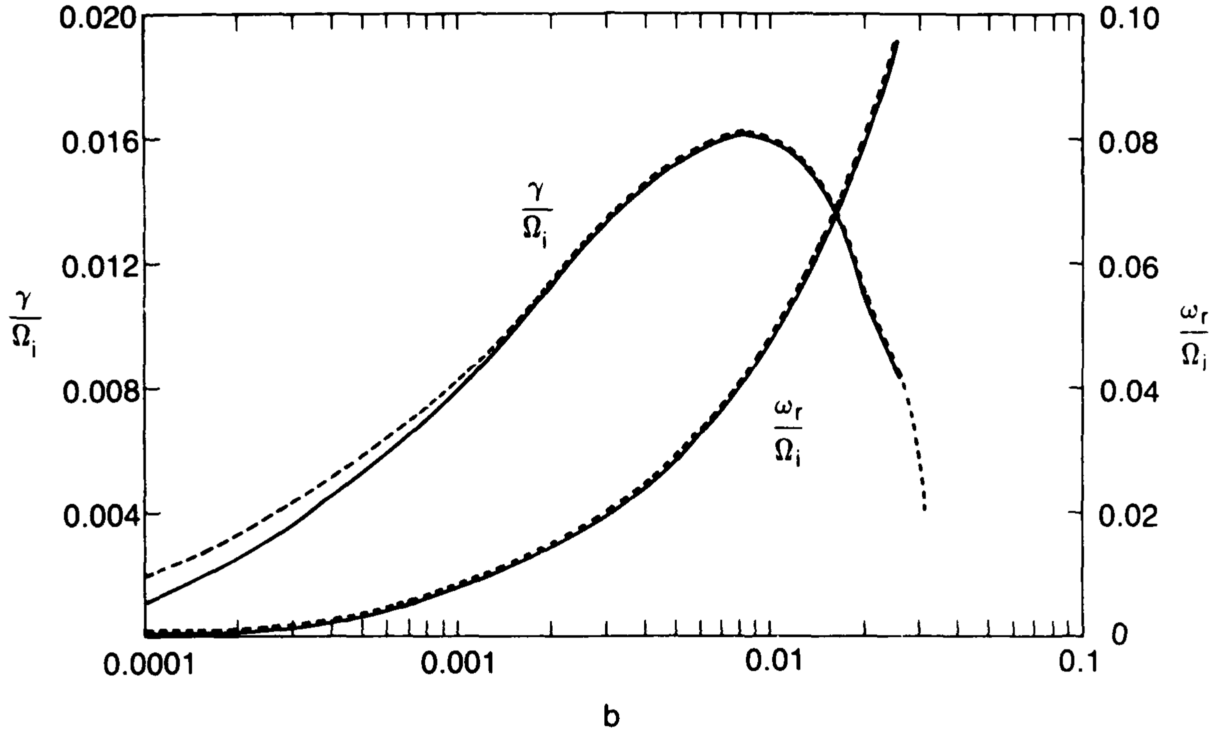

Fig. 2 — The real and imaginary frequencies normalized by Ω_i for the $K-H$ instabilities for the d.c. electric field profile given by $E = E_0 \operatorname{sech}^2(x/L)$ are plotted as a function of b. The solid lines are the eigenvalues of the equation (29) while the dotted lines are the fluid results given in the reference (9). Here $\epsilon = 0.1$, $\tau = 1$, $\mu = 1837$ and $u = 0.0001$.

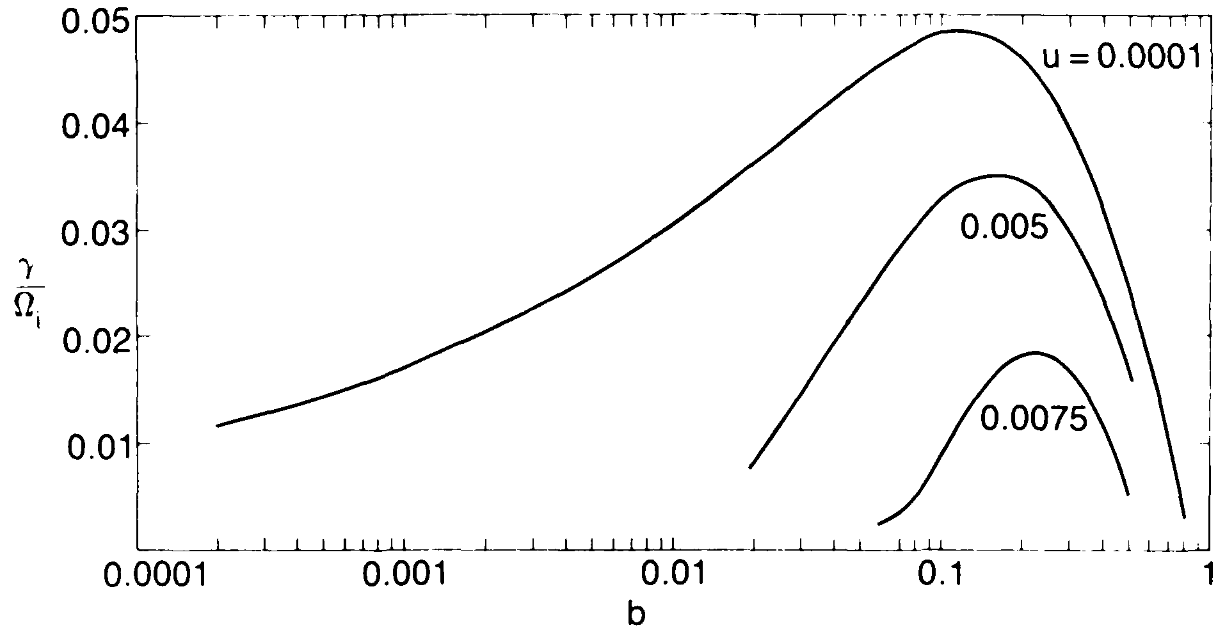

Fig. 3 — A plot of the normalized growth rates of the $K-H$ modes plotted as a function of b for a number of u values. Here $\epsilon = 0.43$, $\mu = 100$ and $\tau = 3.5$.

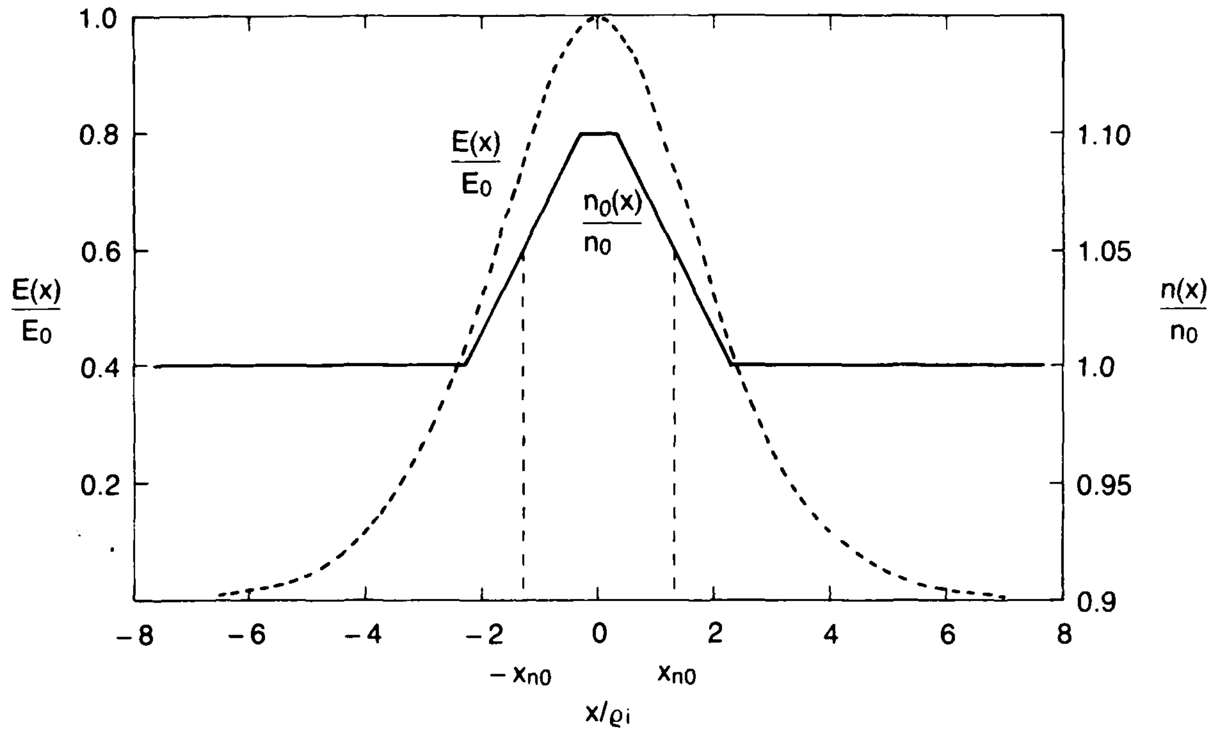

Fig. 4 — The equilibrium field and density configuration used in the calculations of figure (3). Here $x_{n0} = 1.33\rho_i$ $\epsilon_n = -0.05$ when $x_{n0} - \rho_i < x < x_{n0} + \rho_i$ and zero otherwise.

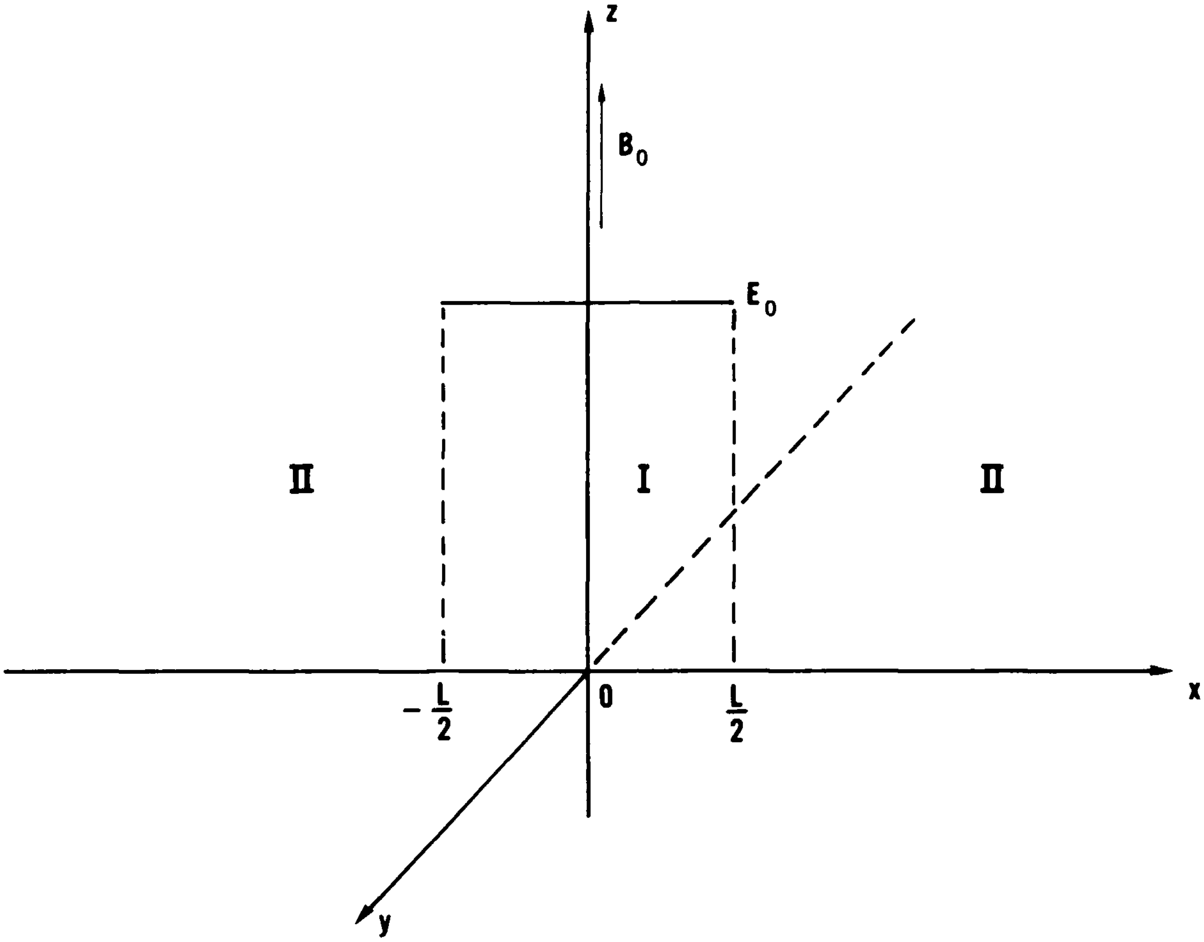

Fig. 5 — A schematic representation of the piecewise continuous d.c. electric field profile.

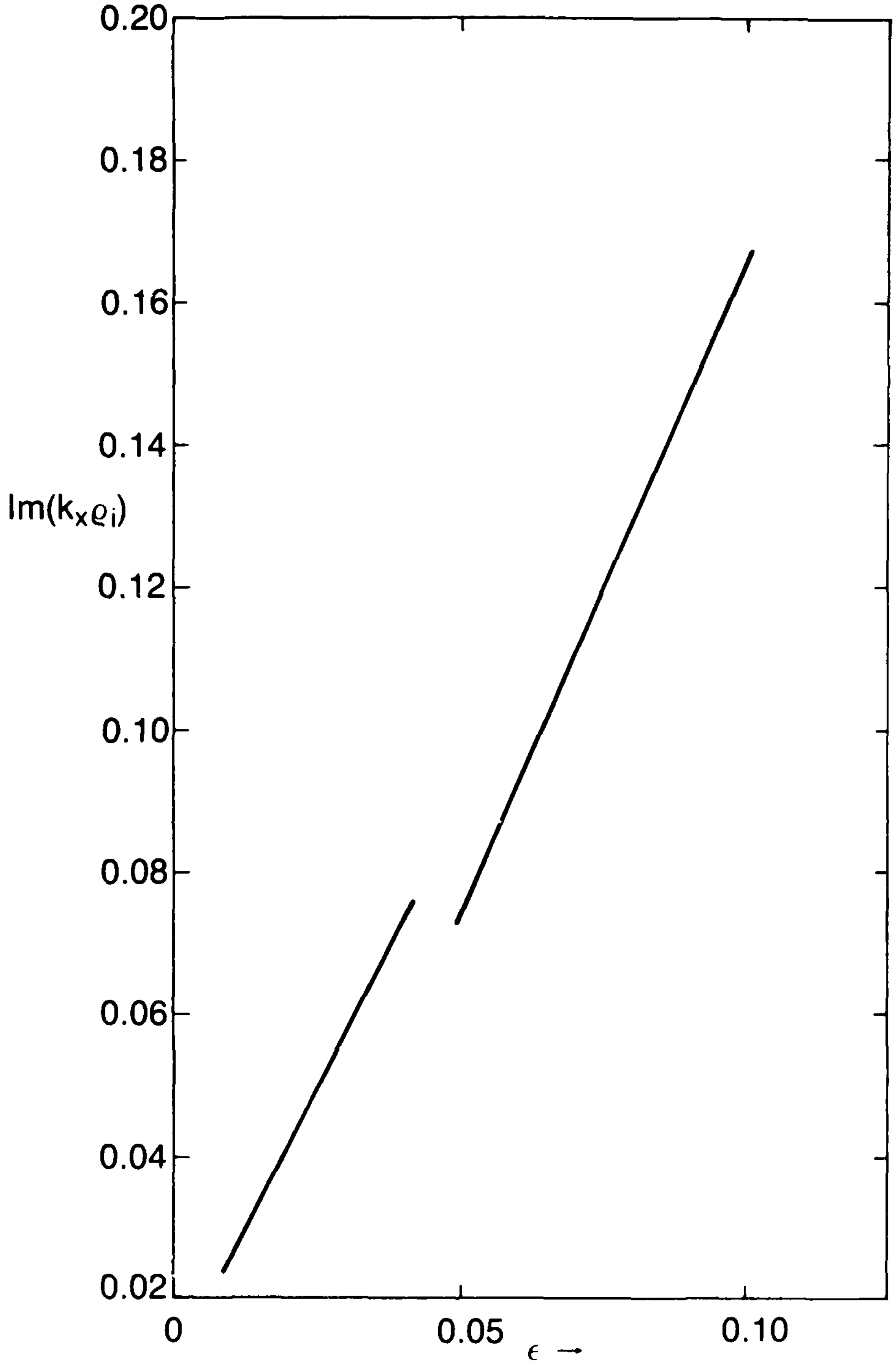

Fig. 6 — A plot of the $\mathrm{Im}(k_x \rho_i)$ against ϵ. The linear dependence confirms the scaling $\gamma / V_G \propto 1/L$. Here $\bar{V}_E = 2.9$, $\tau = 1$, $u = 0.0001$ and $\mu = 1837$.

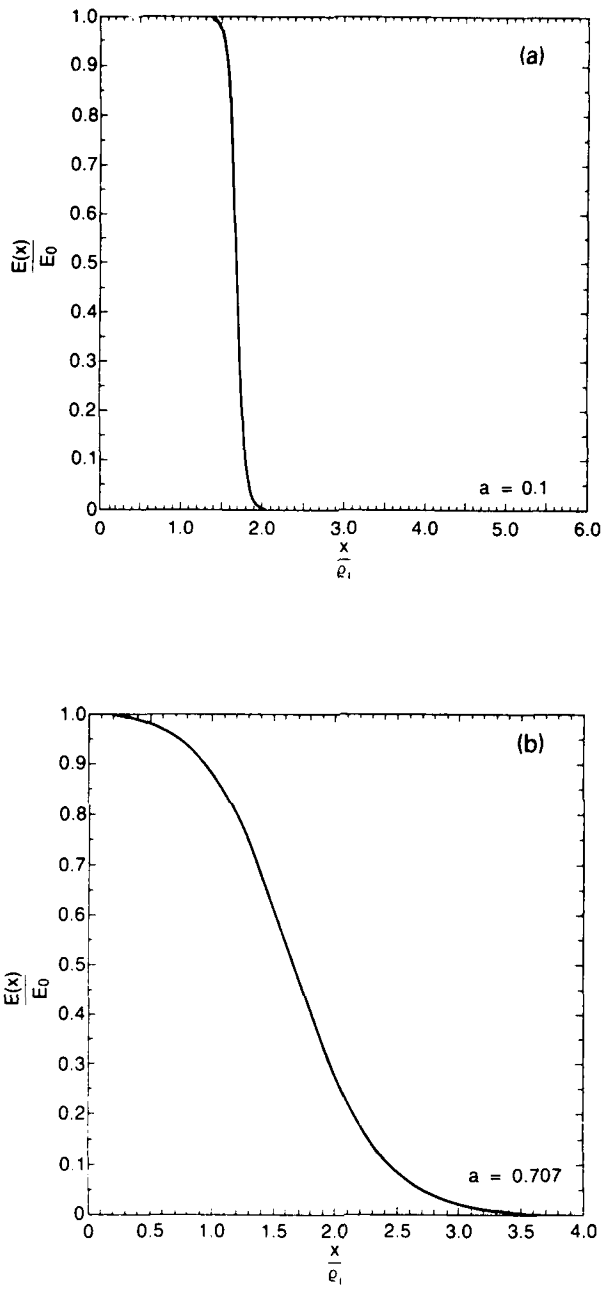

Fig. 7 — The transition from a sharp to a smooth profile given in the equation (39). Here $\epsilon = 0.3$, and (a) $a = 0.1$ and (b) $a = 0.707$.

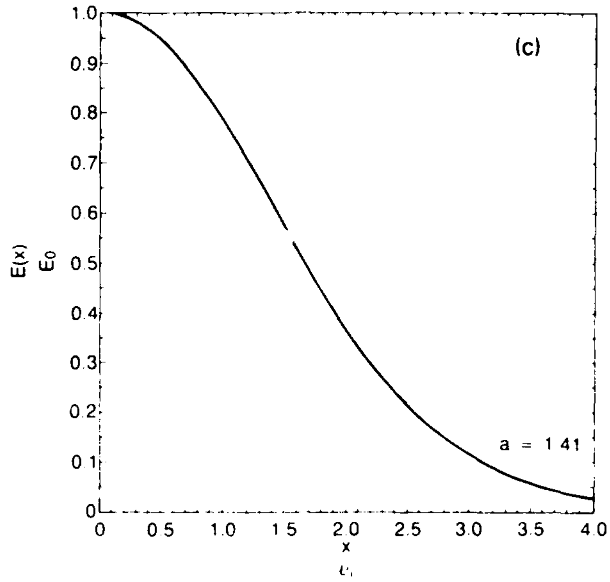

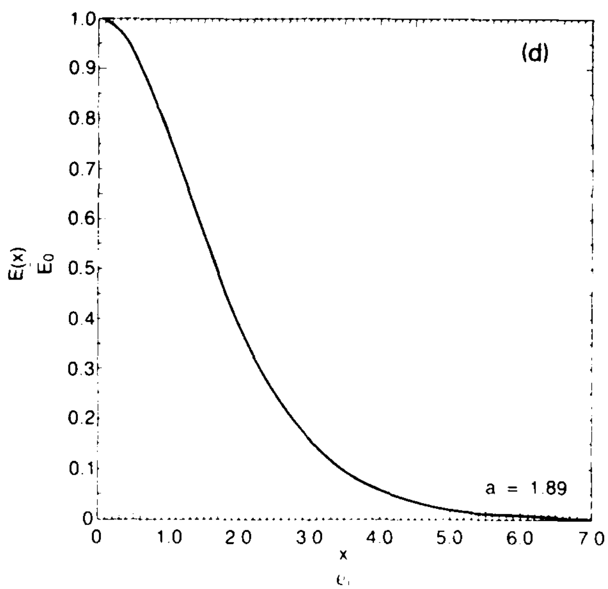

Fig. 7 (Continued) — The transition from a sharp to a smooth profile given in the equation (39). Here $\epsilon = 0.3$, and (c) $a = 1.41$ and (d) $a = 1.89$.

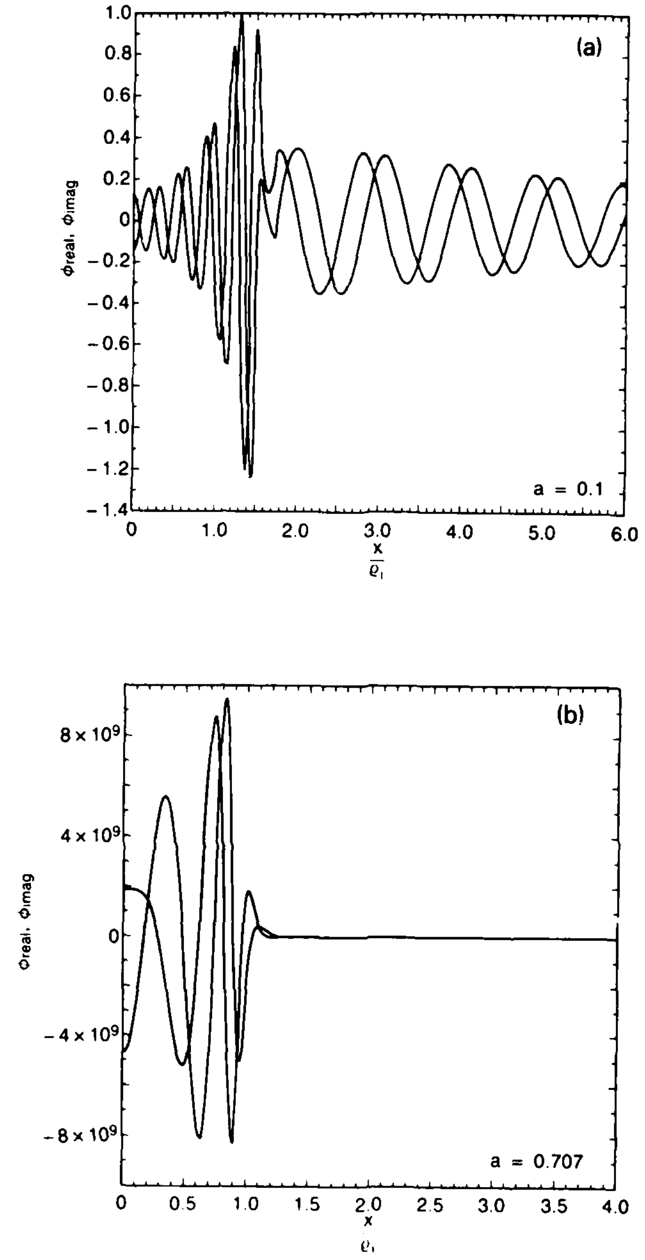

Fig. 8 — The real and imaginary parts of the corresponding eigenfunctions for the profiles in figure (7). Here $b = 8$, $\mu = 1837$, $V_E = 0.6$, $\tau = 3.5$, $u = 0.011$ and $\epsilon_n = -0.07$ if $x_{n0} - 0.9\rho_i < x < x_{n0} + 0.9\rho_i$ and $x_{n0} = 1.66\rho_i$. (a) $a = 0.1$ and (b) $a = 0.707$.

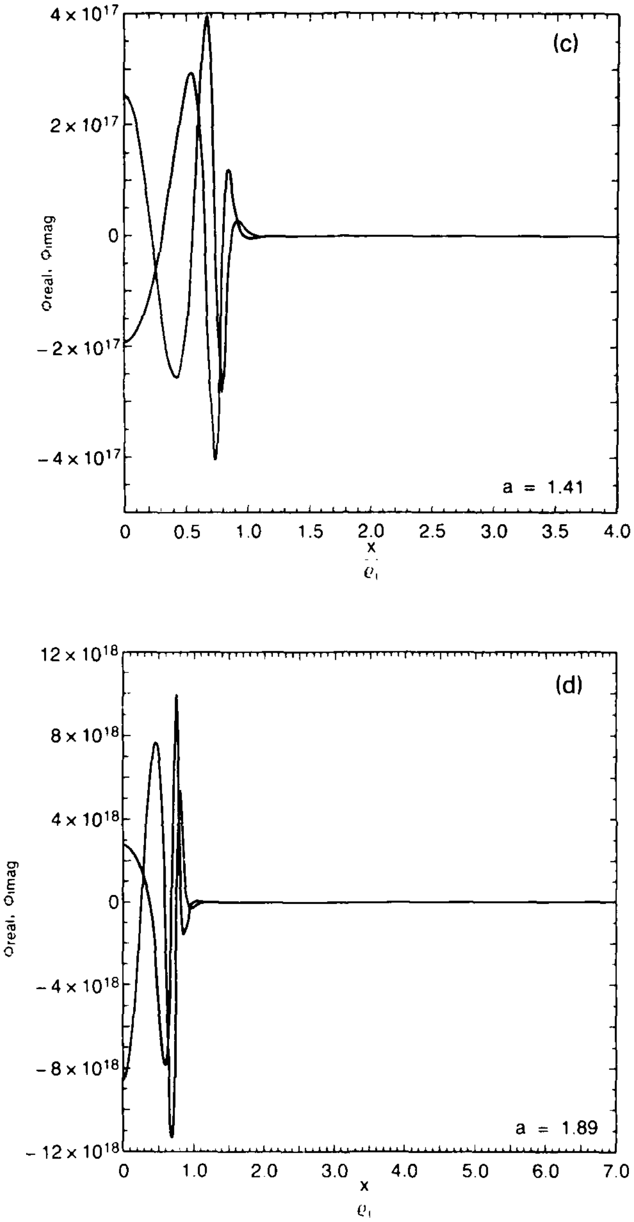

Fig. 8 (Continued) — The real and imaginary parts of the corresponding eigenfunctions for the profiles in figure (7). Here $b = 8$, $\mu = 1837$, $V_E = 0.6$, $\tau = 3.5$, $u = 0.011$ and $\epsilon_n = -0.07$ if $x_{n0} - 0.9_{\rho i} < x < x_{n0} + 0.9_{\rho i}$ and $x_{no} = 1.66_{\rho i}$. (c) $a = 1.41$ and (d) $a = 1.89$.

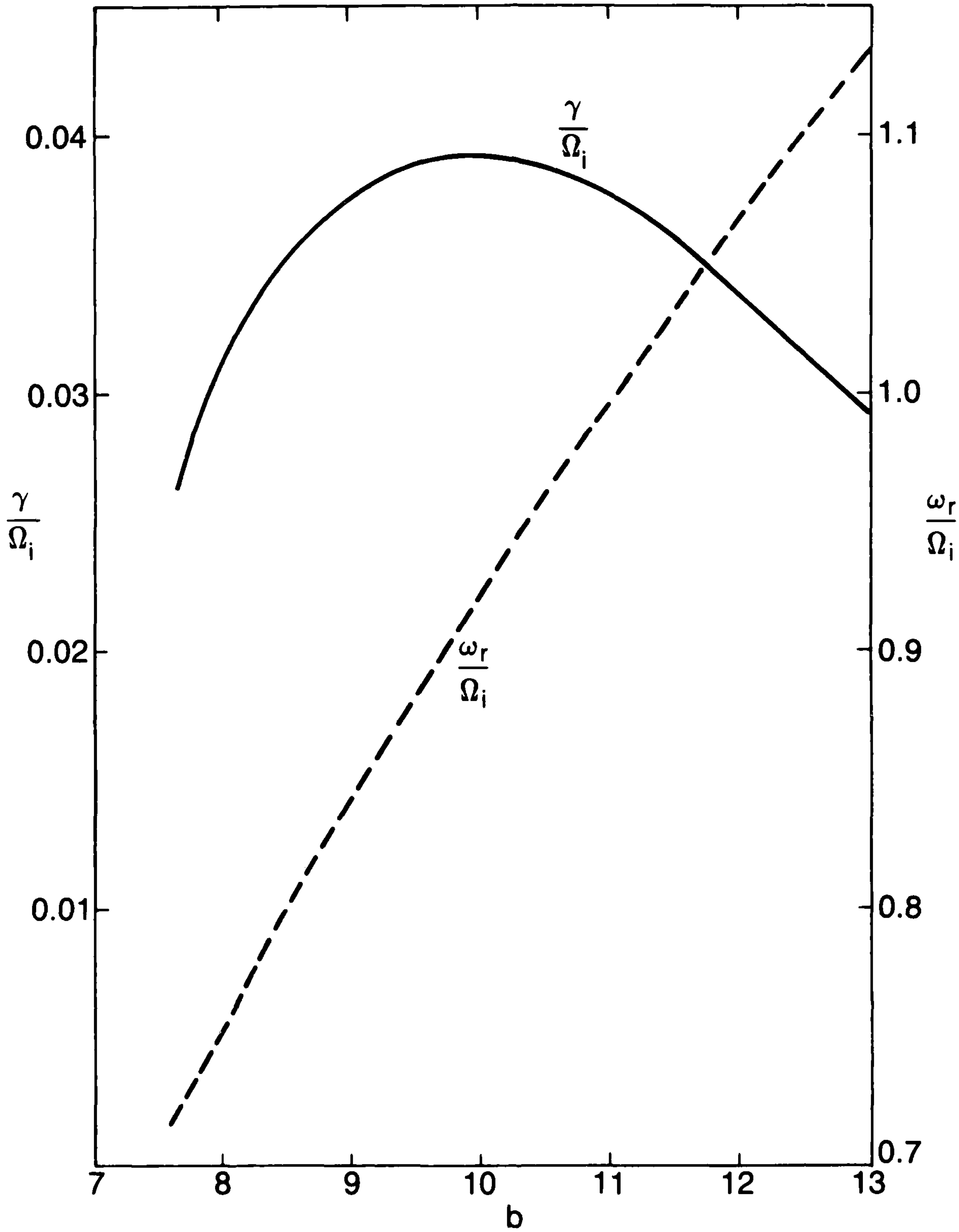

Fig. 9 — A plot of the normalized real and imaginary parts of the eigenfrequency of the ion-cyclotron-like instability against b. Here $\epsilon = 0.3$, $u = 0.011$, $a = 1.87$, $\tau = 3.5$, $\bar{V}_E = 0.6$, $\mu = 1837$ and $\epsilon_n = -0.07$ if $x_{n0} - 0.9\rho_i < x < x_{n0} + 0.9\rho_i$ and zero otherwise and $x_{n0} = 1.66\rho_i$.

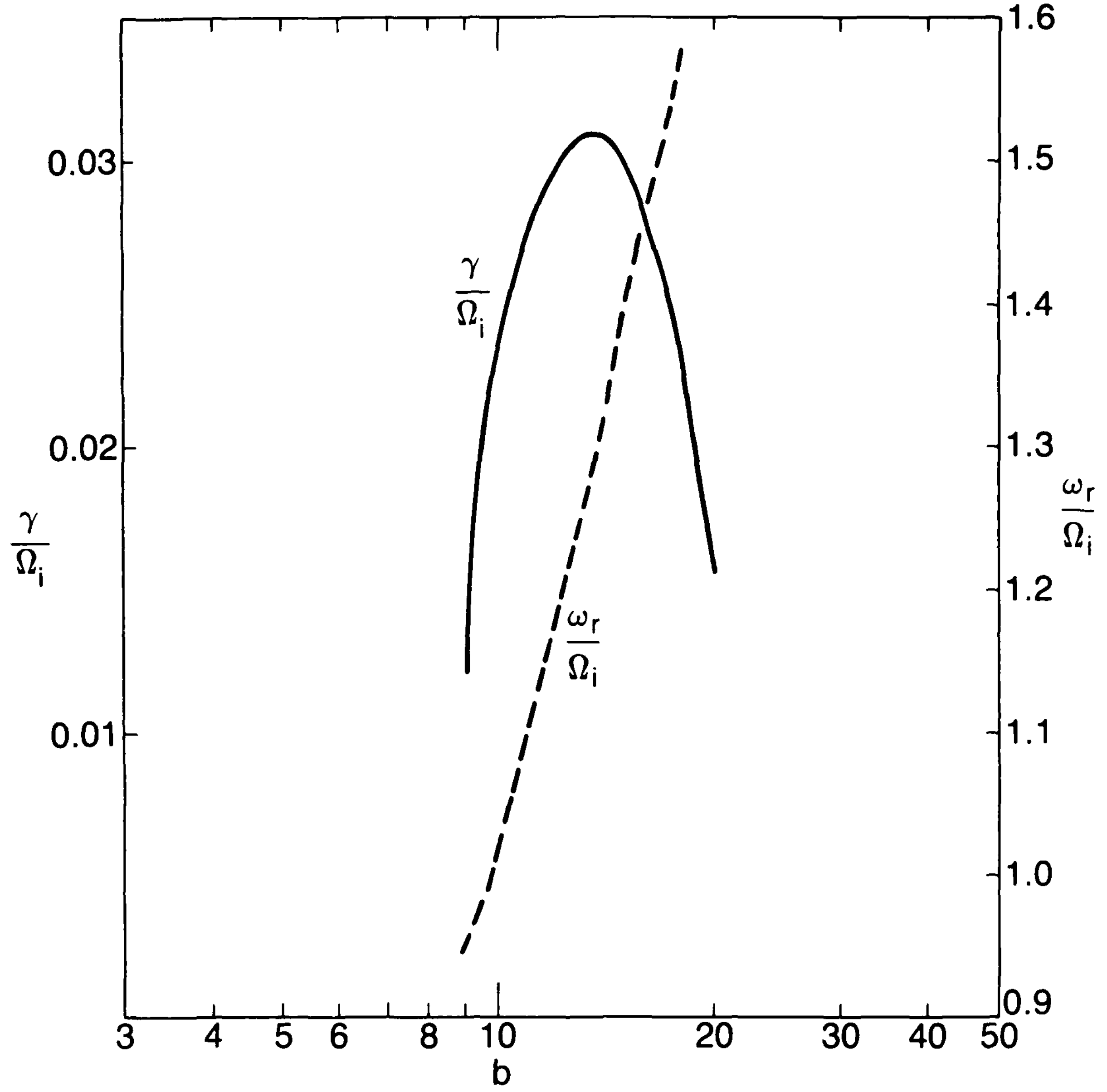

Fig. 10 — A plot similar to the figure (9). Here $u = 0.038$ and rest of the parameters are identical to figure (3).

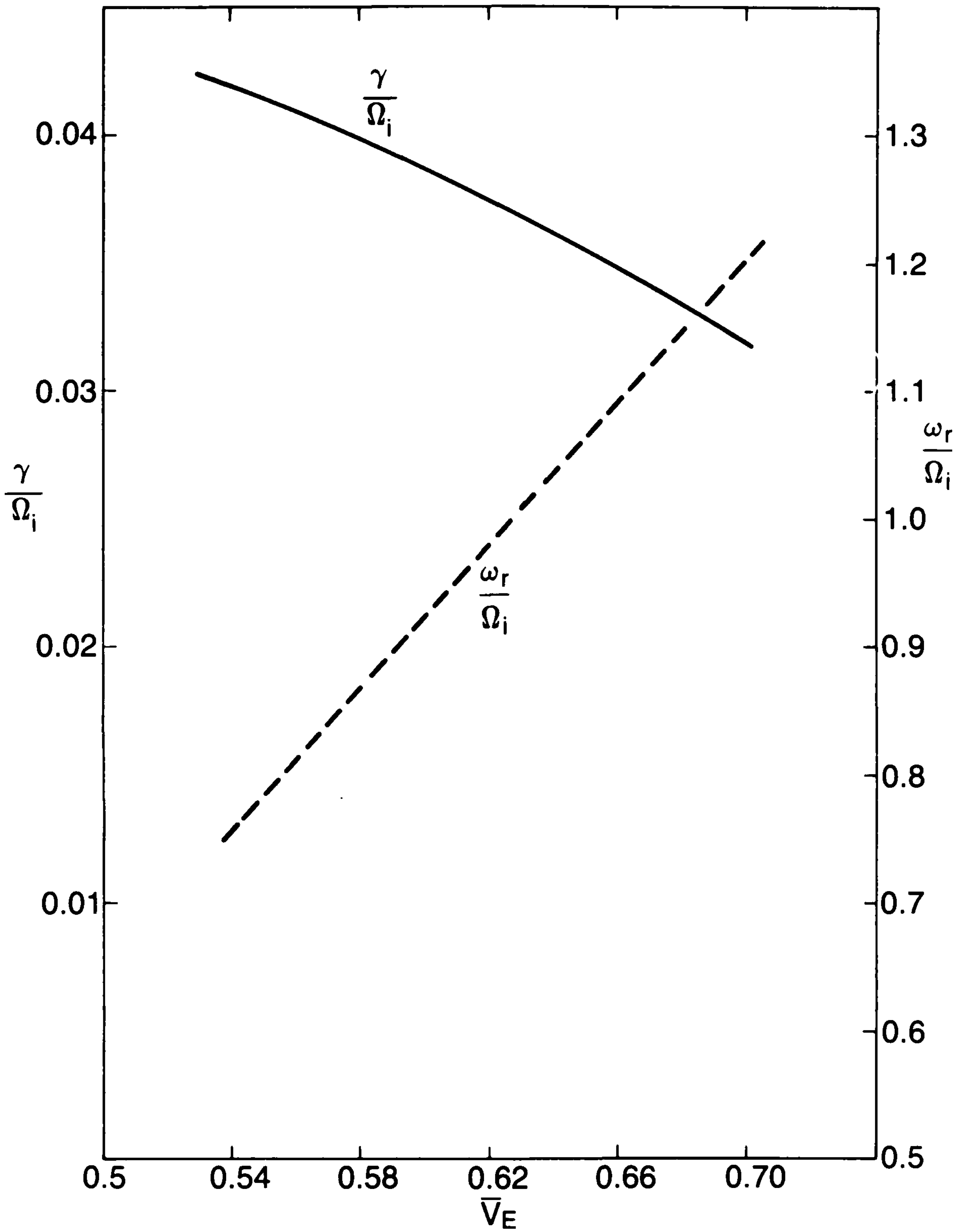

Fig. 11 — The normalized real and imaginary parts of the eigenfrequency of the ion-cyclotron-like waves plotted against $\overline{V}_E$. Here $b = 10$, $\tau = 3.5$, $\mu = 1837$, $u = 0.011$, $\epsilon = 0.3$, $a = 1.87$ and $\epsilon_n = -0.07$ if $x_{n0} - 0.9\rho_i < x < x_{n0} + 0.9\rho_i$ and zero otherwise.

IONOSPHERIC MODELING DISTRIBUTION LIST
(UNCLASSIFIED ONLY)

PLEASE DISTRIBUTE ONE COPY TO EACH OF THE FOLLOWING PEOPLE (UNLESS OTHERWISE NOTED)

NAVAL RESEARCH LABORATORY
WASHINGTON, DC 20375-5000
DR. S. OSSAKOW, CODE 4700 (26 CYS)
DR. I. VITKOVITSKY, CODE 4701
DR. J. HUBA, CODE 4780 (2 CYS)
DR. H. GURSKY, CODE 4100
DR. J.M. GOODMAN, CODE 4180
DR. P. RODRIGUEZ, CODE 4706
DR. P. MANGE, CODE 1004
DR. R. MEIER, CODE 4140
CODE 2628 (22 CYS)
CODE 1220

A.F. GEOPHYSICAL LABORATORY
L.G. HANSCOM FIELD
BEDFORD, MA 01731
DR. T. ELKINS
DR. W. SWIDER
MRS. R. SAGALYN
DR. J.M. FORBES
DR. T.J. KENESHEA
DR. W. BURKE
DR. H. CARLSON
DR. J. JASPERSE
DR. J.F. RICH
DR. N. MAYNARD
DR. D.N. ANDERSON

BOSTON UNIVERSITY
DEPARTMENT OF ASTRONOMY
BOSTON, MA 02215
DR. J. AARONS
DR. M. MENDILLO

CORNELL UNIVERSITY
ITHACA, NY 14850
DR. R. SUDAN
DR. D. FARLEY
DR. M. KELLEY

HARVARD UNIVERSITY
HARVARD SQUARE
CAMBRIDGE, MA 02138
DR. M.B. McELROY

INSTITUTE FOR DEFENSE ANALYSIS
1801 N. BEAUREGARD STREET
ARLINGTON, VA 22311
DR. E. BAUER

MASSACHUSETTS INSTITUTE OF TECHNOLOGY
PLASMA FUSION CENTER
CAMBRIDGE, MA 02139
LIBRARY, NW16-262
DR. T. CHANG
DR. R. LINDZEN

NASA
GODDARD SPACE FLIGHT CENTER
GREENBELT, MD 20771
DR. N. MAYNARD, CODE 696
DR. R.F. BENSON
DR. K. MAEDA
DR. S. CURTIS
DR. M. DUBIN

COMMANDER
NAVAL OCEAN SYSTEMS CENTER
SAN DIEGO, CA 95152
MR. R. ROSE, CODE 5321

NOAA
DIRECTOR OF SPACE AND
ENVIRONMENTAL LABORATORY
BOULDER, CO 80302
DR. A. GLENN JEAN
DR. G.W. ADAMS
DR. K. DAVIES
DR. R.F. DONNELLY

OFFICE OF NAVAL RESEARCH
800 NORTH QUINCY STREET
ARLINGTON, VA 22217
DR. G. JOINER
DR. C. ROBERSON

LABORATORY FOR PLASMA AND
FUSION ENERGIES STUDIES
UNIVERSITY OF MARYLAND
COLLEGE PARK, MD 20742
JEAN VARYAN HELLMAN,
REFERENCE LIBRARIAN

PENNSYLVANIA STATE UNIVERSITY
UNIVERSITY PARK, PA 16802
DR. J.S. NISBET
DR. P.R. ROHRBAUGH
DR. L.A. CARPENTER
DR. M. LEE
DR. R. DIVANY
DR. P. BENNETT
DR. E. KLEVANS

PRINCETON UNIVERSITY
PLASMA PHYSICS LABORATORY
PRINCETON, NJ 08540
DR. F. PERKINS

SAIC
1150 PROSPECT PLAZA
LA JOLLA, CA 92037
DR. D.A. HAMLIN
DR. L. LINSON

SRI INTERNATIONAL
333 RAVENSWOOD AVENUE
MENLO PARK, CA 04025
DR. R. TSUNODA
DR. WALTER CHESNUT
DR. J. VICKREY
DR. R. LIVINGSTON

STANFORD UNIVERSITY
STANFORD, CA 04305
DR. P.M. BANKS
DR. R. HELLIWELL

U.S. ARMY ABERDEEN RESEARCH
AND DEVELOPMENT CENTER
BALLISTIC RESEARCH LABORATORY
ABERDEEN, MD
DR. J. HEIMERL

GEOPHYSICAL INSTITUTE
UNIVERSITY OF ALASKA
FAIRBANKS, AL 99701
DR. L.C. LEE

UTAH STATE UNIVERSITY
4TH AND 8TH STREETS
LOGAN, UT 84322
DR. R. HARRIS
DR. K. BAKER
DR. R. SCHUNK
DR. J. ST.-MAURICE
DR. N. SINGH
DR. B. FEJER

UNIVERSITY OF CALIFORNIA
LOS ALAMOS NATIONAL LABORATORY
EES DIVISION
LOS ALAMOS, NM 87545
DR. M. PONGRATZ, EES-DOT
DR. D. SIMONS, ESS-7, MS-D466
DR. S.P. GARY, ESS-8
DENNIS RIGGIN, ATMOS SCI GROUP

UNIVERSITY OF ILLINOIS
DEPARTMENT OF ELECTRICAL ENGINEERING
1406 W. GREEN STREET
URBANA, IL 61801
DR. ERHAN KUDEKI

UNIVERSITY OF CALIFORNIA,
LOS ANGELES
405 HILLGARD AVENUE
LOS ANGELES, CA 90024
DR. F.V. CORONITI
DR. C. KENNEL
DR. A.Y. WONG

UNIVERSITY OF MARYLAND
COLLEGE PARK, MD 20740
DR. K. PAPADOPOULOS
DR. E. OTT

JOHNS HOPKINS UNIVERSITY
APPLIED PHYSICS LABORATORY
JOHNS HOPKINS ROAD
LAUREL, MD 20810
DR. R. GREENWALD
DR. C. MENG
DR. T. POTEMRA

UNIVERSITY OF PITTSBURGH
PITTSBURGH, PA 15213
DR. N. ZABUSKY
DR. M. BIONDI

UNIVERSITY OF TEXAS AT DALLAS
CENTER FOR SPACE SCIENCES
P.O. BOX 688
RICHARDSON, TX 75080
DR. R. HEELIS
DR. W. HANSON
DR. J.P. McCLURE

DIRECTOR OF RESEARCH
U.S. NAVAL ACADEMY
ANNAPOLIS, MD 21402
(2 CYS)

DISTRIBUTION LIST
(Unclassified Only)

DISTRIBUTE ONE COPY EACH TO THE FOLLOWING PEOPLE (UNLESS OTHERWISE NOTED)

DIRECTOR
NAVAL RESEARCH LABORATORY
WASHINGTON, DC 20375-5000
CODE 4700 (26 CYS)
CODE 4701
CODE 4780 (50 CYS)
CODE 4750 (P. RODRIGUEZ)

OFFICE OF NAVAL RESEARCH
WASHINGTON, DC 22203
C. ROBERSON

DIRECTOR
DEFENSE NUCLEAR AGENCY
WASHINGTON, DC 20305
L. WITTWER
B. PRASAD

COMMANDING OFFICER
OFFICE OF NAVAL RESEARCH
WESTERN REGIONAL OFFICE
1030 EAST GREEN STREET
PASADENA, CA 91106
R. BRANDT

NASA HEADQUARTERS
CODE EE-8
WASHINGTON, DC 20546
S. SHAWHAN
D. BUTLER

NASA/GODDARD SPACE FLIGHT CENTER
GREENBELT, MD 20771
M. GOLDSTEIN, CODE 692
R.F. BENSON, CODE 692
T. NORTHROP, CODE 665
T. BIRMINGHAM, CODE 695.1
A. FIGUERO VINAS, CODE 692
SHING F. FUNG, CODE 696
D.S. SPICER, CODE 682

AEROSPACE CORPORATION
A6/2451, P.O. BOX 92957
LOS ANGELES, CA 90009
A. NEWMAN
D. GORNEY
M. SCHULZ
J. FENNEL

BELL LABORATORIES
MURRAY HILL, NJ 07974
A. HASEGAWA
L. LANZEROTTI

LAWRENCE LIVERMORE LABORATORY
UNIVERSITY OF CALIFORNIA
LIVERMORE, CA 94551
LIBRARY
B. KRUER
J. DEGROOT
B. LANGDON
R. BRIGGS
D. PEARLSTEIN

LOS ALAMOS NATIONAL LABORATORY
P.O. BOX 1663
LOS ALAMOS, NM 87545
S.P. GARY
N. QUEST
J. BRACKBILL
J. BIRN
J. BOROVSKY
D. FORSLUND
J. KINDEL
B. BEZZERIDES
C. NIELSON
E. LINDMAN
D. RIGGIN
D. SIMONS
L. THODE
D. WINSKE

LOCKHEED RESEARCH LABORATORY
PALO ALTO, CA 94303
M. WALT
J. CLADIS
Y. CHIU
R. SHARP
E. SHELLEY

NATIONAL SCIENCE FOUNDATION
ATMOSPHERIC RESEARCH SECTION
WASHINGTON, DC 20550
D. PEACOCK

PHYSICAL INTERNATIONAL CORP.
2400 MERCED STREET
SAN LEANDRO, CA 94557
J. BENFORD
S. STALINGS
Y. YOUNG

SANDIA LABORATORIES
ALBUQUERQUE, NM 87115
A. TOEPFER
D. VANDEVENDER
J. FREEMAN
T. WRIGHT

SCIENCE APPLICATIONS
INTERNATIONAL CORPORATION
LAB. OF APPLIED PLASMA STUDIES
P.O. BOX 2351
LAJOLLA, CA 92037
L. LINSON

TRW SPACE AND TECHNOLOGY GROUP
SPACE SCIENCE DEPARTMENT
BUILDING R-1, ROOM 1170
ONE SPACE PARK
REDONDO BEACH, CA 90278
R. FREDERICKS
W.L. TAYLOR

UNIVERSITY OF ALASKA
GEOPHYSICAL INSTITUTE
FAIRBANKS, AK 99701
LIBRARY
S. AKASOFU
J. KAN
J. ROEDERER
L. LEE
D. SWIFT

UNIVERSITY OF ARIZONA
DEPT. OF PLANETARY SCIENCES
TUCSON, AZ 85721
J.R. JOKIPII

BOSTON COLLEGE
DEPARTMENT OF PHYSICS
CHESTNUT HILL, MA 02167
R.L. CAROVILLANO
P. BAKSHI

UNIVERSITY OF CALIFORNIA, S.D.
LAJOLLA, CA 92037
(PHYSICS DEPARTMENT):
T. O'NEIL
J. WINFREY
LIBRARY
J. MALMBERG
(DEPT. OF APPLIED SCIENCES):
H. BOOKER

UNIVERSITY OF CALIFORNIA
SPACE SCIENCE LABORATORY
BERKELEY, CA 94720
M. TEMERIN
F. MOZER

UNIVERSITY OF CALIFORNIA
PHYSICS DEPARTMENT
IRVINE, CA 92664
LIBRARY
G. BENFORD
N. ROSTOKER
C. ROBERTSON
N. RYNN

UNIVERSITY OF CALIFORNIA
LOS ANGELES, CA 90024
(PHYSICS DEPARTMENT):
J.M. DAWSON
B. FRIED
J. MAGGS
J.G. MORALLES
W. GEKELMAN
R. STENZEL
Y. LEE
A. WONG
F. CHEN
M. ASHOUR-ABDALLA
LIBRARY
J.M. CORNWALL
R. WALKER
P. PRITCHETT
(INSTITUTE OF GEOHPYSICS
AND PLANETARY PHYSICS):
LIBRARY
C. KENNEL
F. CORONITI

UNIVERSITY OF CHICAGO
ENRICO FERMI INSTITUTE
CHICAGO, IL 60637
E.N. PARKER
I. LERCHE
LIBRARY

UNIVERSITY OF COLORADO
DEPT. OF ASTRO-GEOPHYSICS
BOULDER, CO 80302
M. GOLDMAN
LIBRARY

CORNELL UNIVERSITY
SCHOOL OF APPLIED AND
ENGINEERING PHYSICS
COLLEGE OF ENGINEERING
ITHACA, NY 14853
LIBRARY
R. SUDAN
B. KUSSE
H. FLEISCHMANN
C. WHARTON
F. MORSE
R. LOVELACE
P.M. KINTNER

HARVARD UNIVERSITY
CENTER FOR ASTROPHYSICS
60 GARDEN STREET
CAMBRIDGE, MA 02138
G.B. FIELD
R. ROSNER
K. TSINGANOS
G.S. VAIANA

UNIVERSITY OF IOWA
IOWA CITY, IA 52240
C.K. GOERTZ
D. GURNETT
G. KNORR
D. NICHOLSON
C. GRABBE
L.A. FRANK
K. NISHIKAWA
N. D'ANGELO
R. MERLINO
C. HUANG

UNIVERSITY OF MARYLAND
PHYSICS DEPARTMENT
COLLEGE PARK, MD 20742
K. PAPADOPOULOS
H. ROWLAND
C. WU

UNIVERSITY OF MARYLAND, IPST
COLLEGE PARK, MD 20742
DAVID MATTHEWS

UNIVERSITY OF MINNESOTA
SCHOOL OF PHYSICS
MINNEAPOLIS, MN 55455
LIBRARY
J.R. WINCKLER
P. KELLOGG
R. LYSAK

M.I.T.
CAMBRIDGE, MA 02139
LIBRARY
(PHYSICS DEPARTMENT):
B. COPPI
V. GEORGE
G. BEKEFI
T. CHANG
T. DUPREE
R. DAVIDSON
(ELECTRICAL ENGINEERING
DEPARTMENT):
R. PARKER
A. BERS
L. SMULLIN
(R.L.E):
LIBRARY
(SPACE SCIENCE):
READING ROOM

UNIVERSITY OF NEW HAMPSHIRE
DEPARTMENT OF PHYSICS
DURHAM, NH 03824
R.L. KAUFMAN
J. HOLLWEG

PRINCETON UNIVERSITY
PRINCETON, NJ 08540
PHYSICS LIBRARY
PLASMA PHYSICS LAB. LIBRARY
F. PERKINS
T.K. CHU
H. OKUDA
H. HENDEL
R. WHITE
R. KURLSRUD
H. FURTH
S. YOSHIKAWA
P. RUTHERFORD

RICE UNIVERSITY
HOUSTON, TX 77001
SPACE SCIENCE LIBRARY
T. HILL
R. WOLF
P. REIFF
G.-H. VOIGT

UNIVERSITY OF ROCHESTER
ROCHESTER, NY 14627
A. SIMON

STANFORD UNIVERSITY
RADIO SCIENCE LABORATORY
STANFORD, CA 94305
R. HELLIWELL

STEVENS INSTITUTE OF TECHNOLOGY
HOBOKEN, NJ 07030
B. ROSEN
G. SCHMIDT
M. SEIDL

UNIVERSITY OF TEXAS
AUSTIN, TX 78712
W. DRUMMOND
V. WONG
D. ROSS
W. HORTON

UNIVERSITY OF TEXAS
CENTER FOR SPACE SCIENCES
P.O. BOX 688
RICHARDSON, TX 75080
DAVID KLUMPAR

THAYER SCHOOL OF ENGINEERING
DARTMOUTH COLLEGE
HANOVER, NH 03755
BENGT U.O. SONNERUP
M. HUDSON

UTAH STATE UNIVERSITY
DEPT. OF PHYSICS
LOGAN, UT 84322
ROBERT W. SCHUNK

UNIVERSITY OF THESSALONIKI
DEPARTMENT OF PHYSICS
GR-54006 THESSALONIKI,
GREECE
L. VLAHOS

Records 1 copy

END
DATE
FILMED
DTIC
JULY 88